Structures 51 (2023) 640–656

Contents lists available at ScienceDirect

Structures

journal homepage: www.elsevier.com/locate/structures

Seismic protection of land-based wind turbine towers using the tuned inerter damper

Gioacchino Alotta [a], Chiara Biondo [a], Agathoklis Giaralis [b,c,d], Giuseppe Failla [a,*]

[a] Department of Civil, Energy, Environmental and Materials Engineering (DICEAM), University of Reggio Calabria, Via Graziella, 89124 Reggio Calabria, Italy
[b] Department of Engineering, City, University of London, London, UK
[c] ABL Group, London, UK
[d] Department of Civil Infrastructure & Environmental Engineering, Khalifa University, Abu Dhabi, United Arab Emirates

ARTICLE INFO

Keywords:
Tuned inerter damper
Finite element inerter modelling
Land-based wind turbine
Seismic response mitigation
Passive vibration control

ABSTRACT

The tuned inerter damper (TID) has recently emerged in the literature as a bona fide resonant vibration absorber for the seismic protection of building structures by relaxing the requirement for large secondary mass employed in conventional tuned mass dampers (TMDs). This is achieved by leveraging the inertia property of lightweight inerter devices, called inertance. This paper extends the application of the TID to address the seismic response reduction of the supporting towers of land-based wind turbines (WTs). To this aim, a novel vibration suppression strategy is proposed for WT towers in which a TID is attached at two different locations inside and along the height of the tower and is tuned to the tower's dominant natural frequency. Numerical assessment is supported by developing a finite-element model of the benchmark NREL 5 MW WT equipped with an ad hoc TID model placed at different locations in the tower and with different inertance values. The assessment includes time-domain response history analyses for 28 earthquake ground motions (GMs) with and without pulses under concurrent thrust wind forces for 4 different mean wind speeds. Improved TID vibration suppression performance is noted by installing the TID closer to the tower top and by increasing the inertance and/or the distance of the attachment locations. Further, the TID achieves significant reductions of tower top peak displacement and acceleration as well as peak base shear and bending moment for all the different combinations of GMs and wind speeds, outperforming a conventional TMD with 5% secondary mass ratio placed in the nacelle.

1. Introduction

In the last decade, wind renewable energy harnessed by wind turbine farms became an important and strategic alternative to fossil energy sources, playing a key role in the clean energy transition worldwide. New wind farms are continuously developed worldwide comprising horizontal axis wind turbines (WTs) with evermore larger rotors supported by taller towers to harness higher energy wind at higher altitudes, aiming to accommodate the increasing demands in renewable energy. Consequently, WT towers become more susceptible to excessive vibrations under environmental dynamic loads which reduce the energy generation potential of wind farms and may ultimately lead to catastrophic failures [1]. In this regard, vibration mitigation of WT towers is critical for the development of robust and reliable wind energy generation and technology [2,3]. This is a particularly relevant issue in high seismicity areas as earthquake-induced vibrations pose high demands to WT towers [4–6], potentially causing structural damage, thus increasing maintenance costs and incurring long periods of downtime (inactivity of WT energy converter) with consequent reduced renewable energy production.

In this context, various types of passive resonant vibration absorbers including tuned mass dampers (TMDs) [7–9] and tuned liquid column dampers (TLCDs) [10,11] were widely studied in the literature for mitigating wind-borne oscillations in land-based WTs and in offshore WTs, as well as wave-induced motions in offshore floating WTs and earthquake-induced vibrations in bottom-fixed WTs. Further, the use of TMDs for the task at hand was taken up by the industry [12]. TMDs utilize the inertia of additive free-to-oscillate secondary mass blocks, commonly hanged as pendula from inside the WT tower top (e.g. [13,14]) or housed within the WT nacelle (e.g. [7,8,12]), to counterbalance the structural oscillations through resonance (tuning) to specific structural modes of vibration and to dissipate kinetic energy through

* Corresponding author.
E-mail address: giuseppe.failla@unirc.it (G. Failla).

https://doi.org/10.1016/j.istruc.2023.03.004
Received 18 October 2022; Received in revised form 28 February 2023; Accepted 1 March 2023

Table 1
Main geometrical and mass properties of NREL 5 MW HAWT [27].

Property	Value	Unit
Rotor diameter D	126	m
Rotor center of mass height h_R	90	m
Blade mass	17,740	kg
Hub mass	56,780	kg
Nacelle mass	240,000	kg
Rotor-Nacelle-Assembly (RNA) mass	350,000	kg
Cut-in wind speed U_i	3.0	m/s
Cut-out wind speed U_o	25.0	m/s
Rated wind speed U_r	11.4	m/s
Rated power	5	MW

Table 2
Main geometrical and mass properties of the support tower [27].

Property	Value	Unit
Tower height H	87.6	m
Tower base diameter	6.0	m
Tower base thickness	0.027	m
Tower top diameter	3.87	m
Tower top thickness	0.019	m

dissipative damping elements (e.g. fluid viscous dampers) connecting the TMD mass to the WT structure. Alternatively, TLCDs utilize the inertia of moving liquids inside tubes tuned to counterbalance structural oscillations and to dissipate kinetic energy using orifices installed inside the tubes (e.g. [10]). However, TLCDs exhibit nonlinear behavior and thus accurate modelling and parameter calibration under different levels of excitation are challenging. On the other end, TMDs are easier to tune. Nevertheless, the motion control effectiveness of TMDs is limited by the dead weight of the secondary mass that needs to be accommodated by the tower as well as by space restrictions in the WT tower or nacelle in accommodating the relative displacement (stroke) of the secondary mass. In fact, TMD weight and stroke accommodation requirements become rather critical when targeting the low-frequency side-side or fore-aft tower modes, especially under seismic excitations [13,15], which render their use for seismic protection of WT towers less favorable in practical applications.

To this end, various inerter-based resonant vibration absorbers (IVAs) were recently considered for vibration mitigation and motion control of WT towers [16–18], prompted by the fact that IVAs have significantly reduced requirements for secondary mass and stroke, compared to TMDs. This is achieved by leveraging the mass and/or the rotational motion amplification attribute of inerters. Specifically, the inerter was theoretically defined by Smith [19], as a linear massless mechanical element resisting relative acceleration through its inertance property, b, measured in mass units (kg). Further, inerter devices with inertance several orders of magnitude higher than their physical mass were devised based on mechanisms transforming, through gearing, the slow translational relative motion at the device ends into fast rotational motion of a flywheel (i.e. a lightweight fast-spinning disk) [20], among several alternative technologies [21,22]. In this regard, the study in ref. [23] presented an IVA termed tuned viscous mass damper (TVMD), currently used for the seismic protection of a handful of buildings in Japan [20], which uses an inerter mechanism as a rotational motion amplifier to enhance the damping efficiency of a viscous damper together with a soft-spring connection. The latter spring is tuned such that the TVMD suppresses (targets) a single structural vibration mode. The authors of ref. [24] replaced the linear viscous damping element of the conventional TMD by a TVMD, thus devising an IVA called rotational inertia tuned mass damper (RITMD) with superior performance compared to the TMD. The potential of a RITMD mounted in the nacelle was studied in ref. [17] for the seismic response mitigation of land-based WTs, in ref. [25] for suppressing wind-borne oscillations in land-based WTs, and in ref. [26] for motion control of floating WTs. Furthermore, the authors of ref. [16] assessed the performance of RITMD vis-à-vis two alternative IVA configurations, all mounted in the nacelle, for motion control of the benchmark 5 MW NREL WT [27] on a barge floating

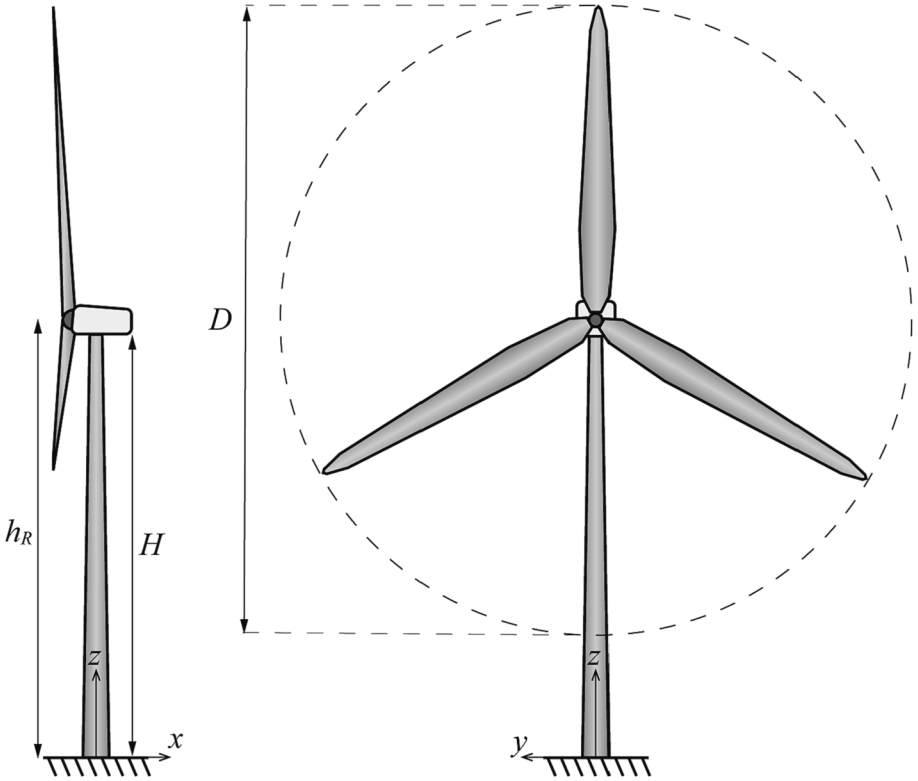

Fig. 1. Main geometrical properties of wind turbine under study and coordinate system.

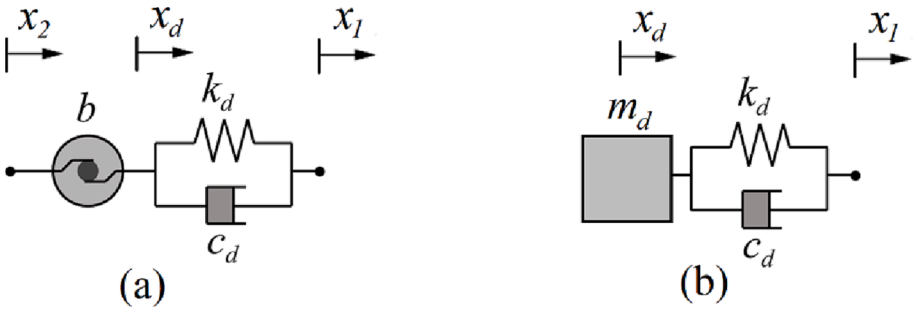

Fig. 2. (a) Tuned inerter damper (TID), (b) Tuned mass damper (TMD).

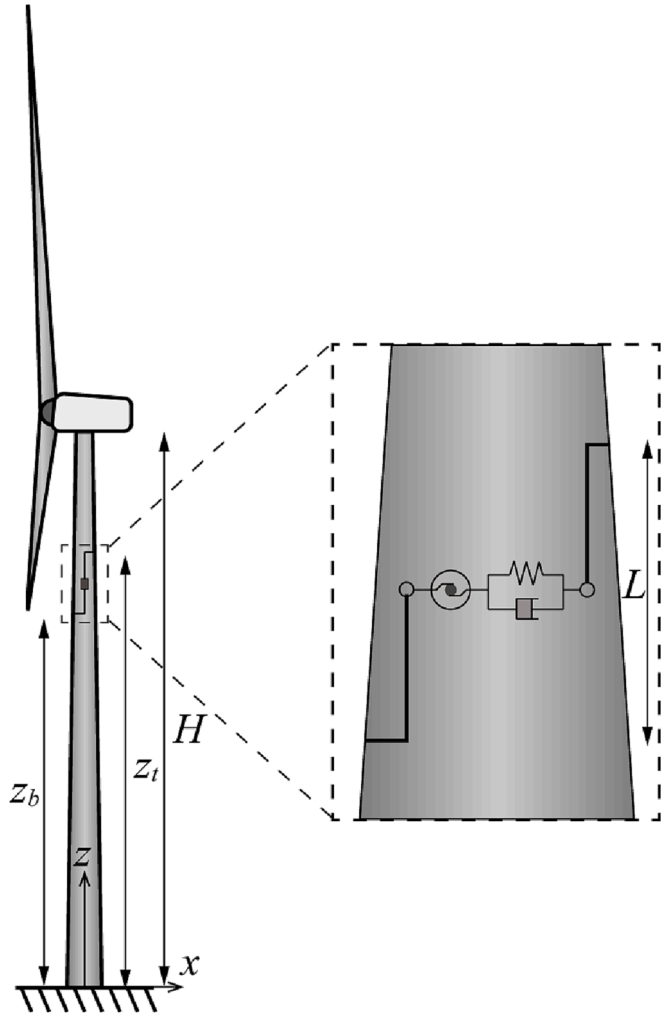

Fig. 3. Wind turbine under study, equipped with the TID.

platform. More recently, the authors of ref. [28] employed passive network synthesis approaches to derive and tune various IVA configurations placed in the nacelle for motion control of floating WTs and for seismic protection of land-based WTs, respectively.

Notably, all the above reviewed studies considered IVAs with one attachment point, similar to the conventional TMD, placed in the nacelle of WTs. Indeed, significantly less research work was devoted on exploring the potential of lightweight IVAs with two attachment points such as the tuned inerter damper (TID) [29] and the tuned mass damper inerter (TMDI) [30], for WT motion control. This is so, despite the fact that these IVAs were shown to be much more effective than TMDs in mitigating lateral vibrations in tall slender cantilevered structures,

Table 3
Properties of the considered TID layouts.

Layout	b (t)	L	z_t (Position)
1	500	$H/10$	$3/5H$ (P1)
2	500	$H/10$	$4/5H$ (P2)
3	500	$H/10$	H (P3)
4	500	$H/5$	$3/5H$ (P1)
5	500	$H/5$	$4/5H$ (P2)
6	500	$H/5$	H (P3)
7	1000	$H/10$	$3/5H$ (P1)
8	1000	$H/10$	$4/5H$ (P2)
9	1000	$H/10$	H (P3)
10	1000	$H/5$	$3/5H$ (P1)
11	1000	$H/5$	$4/5H$ (P2)
12	1000	$H/5$	H (P3)

including high-rise buildings under earthquake [31,32] and wind loads [33–35] by attaching them to different building floors. One exception is the work [18], in which a TMDI attached between the nacelle and a lower location within the tower was considered for motion control of floating WTs. Further, the authors of ref. [36] studied the potential of the TID to mitigate the dynamic response of offshore jackets (lattice truss-work structures), widely used as bottom-fixed foundations of offshore WTs, under combined earthquake and ocean wave loads.

To this end, this paper innovates by considering, for the first time in the literature, the use of a lightweight two attachment point IVA for the seismic response mitigation of land-based WT towers, accounting for simultaneous wind action. Specifically, the use of a TID is herein proposed for the task, attached at two different locations inside and along the height of the WT tower. The TID is tuned to the first natural frequency of the WT tower along the fore-aft direction using a practically meritorious structure-specific H_∞-style tuning, given the complexity and uncertainty of the combined wind plus earthquake excitations. The seismic vibration suppression potential of the TID is numerically assessed by developing a finite element (FE) model of the baseline NREL 5 MW wind turbine [27] implemented in SAP2000 software [37], including an ad hoc model of the TID. The assessment includes the derivation of frequency response functions as well as comprehensive time-domain response history analyses for several pulse-like and non-pulse-like earthquake records under the concurrent action of thrust wind forces for different mean wind speed conditions. Attention is focused on gauging the influence of the location of the two TID attachment points onto the tower, their distance, as well as the TID inertance on the level of seismic response mitigation in terms of peak tower top displacement, acceleration, base shear, base bending moment, and TID stroke. Comparisons are also drawn against a standard TMD placed in the nacelle of the adopted benchmark WT. The presentation begins by describing the case study WT structure, with the proposed TID configuration and their FE modelling.

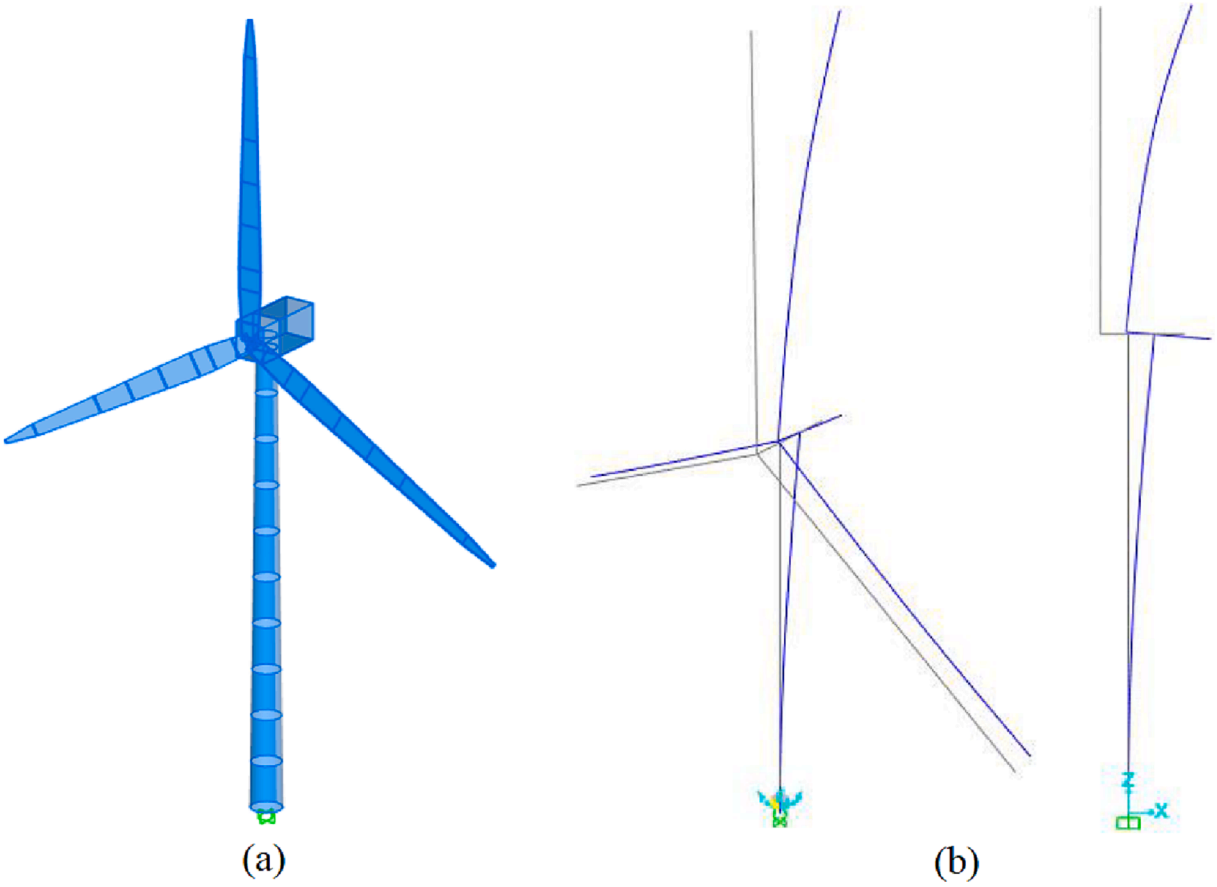

Fig. 4. (a) Schematic of the FE model of the WT system in Tables 1 and 2, (b) First WT tower fore-aft mode shape in 3D view and in side view (Grey line: undeformed shape; blue line: deformed shape). (For interpretation of the references to colour in this figure legend, the reader is referred to the web version of this article.)

Table 4
Natural frequencies of the unprotected wind turbine, as obtained from the SAP2000 FE model in Fig. 4, compared with those obtained from FAST and ABAQUS in ref. [39]. Frequency values in Hz.

Mode number	SAP2000	FAST	ABAQUS	Mode description
1	0.32	0.32	0.32	1st tower fore-aft
2	0.32	0.31	0.31	1st tower side-to-side
3	0.59	0.67	0.63	1st blade asymmetric flapwise yaw
4	0.61	0.67	0.66	1st blade asymmetric flapwise pitch
5	0.63	0.70	0.69	1st blade collective flap
6	1.02	1.08	1.05	1st blade asymmetric edgewise pitch
7	1.11	1.09	1.07	1st blade asymmetric edgewise yaw
8	1.50	1.93	1.70	2nd blade asymmetric flap yaw
9	1.69	1.92	1.83	2nd blade asymmetric flap pitch
10	1.81	2.02	1.93	2nd blade collective flap
11	2.55	2.90	2.78	2nd tower fore-aft
12	2.72	2.94	2.83	2nd tower side-side

2. Case study wind turbine equipped with tuned inerter damper

2.1. Description of wind turbine with tuned inerter damper configuration

The baseline NREL 5 MW horizontal axis WT developed in [27] is herein considered to study and assess the effectiveness of the TID configuration for seismic protection of onshore WTs. The adopted benchmark WT has been widely utilized in the literature to study the seismic response of WTs to earthquakes (e.g. [38–40]). Key geometric and mass properties of the NREL 5 MW WT are summarized in Table 1, along with the critical mean wind speed values which delimit the different operational stages of the WT. These values include the cut-in speed below which no power is generated, the rated speed at and above which the WT blades pitch control system is activated to rotate the blades so that generated power remains constant and equal to the rated power, and the cut-out speed at which the turbine shuts off to minimize risk of damage.

The adopted WT is supported by a tapered steel tower [27] assumed to be fixed at the base. The geometrical properties of the tower are provided in Table 2, while its mass properties are determined by taking the material mass density equal to 8500 kg/m^3 which is larger than the typical range of values for constructional steel to account for paint, bolts, welds and flanges which are not considered in the nominal thickness of the tower cross-section [27]. A sketch of the adopted land-based WT system is shown in Fig. 1.

For seismic protection of the WT, it is herein proposed to equip the tower with a TID. The TID, originally proposed in ref. [29], is a linear passive IVA modelled by a spring with stiffness k_d linked in parallel with a dashpot (e.g. a linear fluid viscous damper) with damping coefficient c_d which are further connected in series with an inerter, as shown in Fig. 2(a). Therefore, in the TID, the inerter develops a force given as

$$F(t) = b\left(\ddot{x}_d(t) - \ddot{x}_2(t)\right) \tag{1}$$

where $x_d(t)$ and $x_2(t)$ are the displacements at the two ends of the inerter element as indicated in Fig. 2(a) and a dot over a symbol denotes differentiation with respect to time t. Notably, if the leftmost end of the inerter is grounded (i.e. $x_2 = 0$), then the TID behaves exactly as a

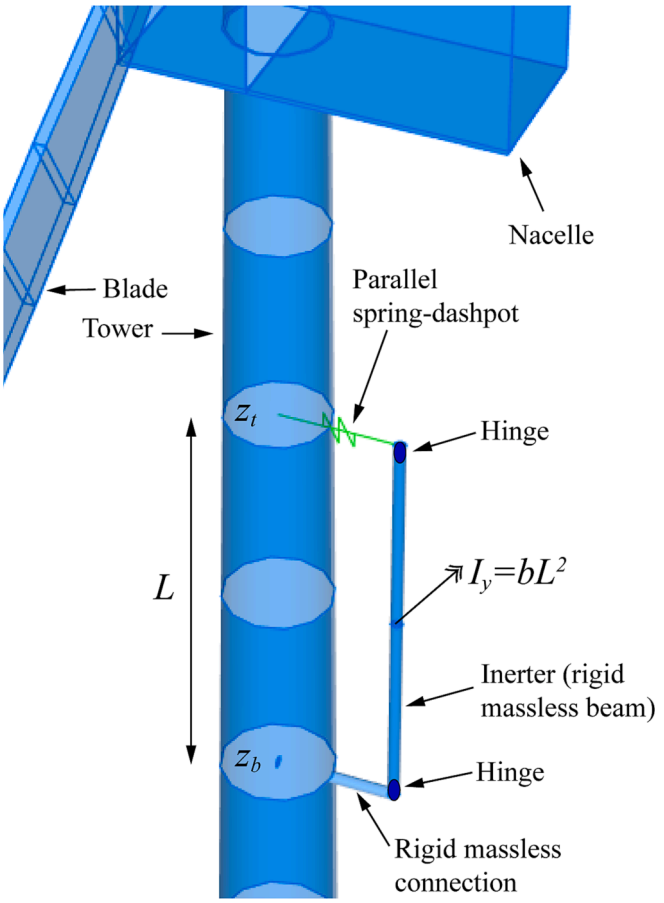

Fig. 5. Implementation of the TID in SAP2000 commercial FE software package.

Table 5
Calibration parameters obtained for each set of input parameters in Table 3 and for the 35 t TMD.

Layout	k_d (kN/m)	c_d (kNs/m)	ω_d (rad/s)	ζ_d
1	1913.3	162.2	1.956	0.083
2	1874.4	211.4	1.936	0.109
3	1842.4	243.6	1.920	0.127
4	1797.1	281.7	1.896	0.149
5	1666.2	364.2	1.825	0.200
6	1552.9	416.1	1.762	0.236
7	3723.5	449.5	1.930	0.116
8	3576.2	577.1	1.891	0.153
9	3458.4	657.0	1.860	0.177
10	3296.7	746.8	1.816	0.206
11	2859.1	918.4	1.691	0.272
12	2513.9	1004.3	1.586	0.317
35 t TMD	119.2	24.1	1.845	0.187

standard linear passive TMD, shown in Fig. 2(b), with secondary mass m_d equal to the inertance b. Meanwhile, it is further noted that the inertance can readily scale up independently of the physical mass/weight of inerter devices as demonstrated through physical testing of various prototypes using mechanical gearing [20] or hydraulic pumps [21]. In this regard, the inertance in the TID can be taken several orders of magnitude larger than the device mass. Therefore, the significant advantage of the TID over the conventional TMD is that it employs large inertial effects in suppressing structural vibrations without imposing large additive dead load or attracting significant mass-proportional seismic forces during an earthquake.

Still, unlike the TMD, the TID requires two attachment points. Given that a ground support is not practical in the case of WT towers, it is herein proposed to attach the TID between two different locations inside the WT tower, as depicted in Fig. 3, to mitigate earthquake induced ground motions in the fore-aft direction, accounting for the wind thrust force. The distance between the two TID attachment locations along the tower height is $L = z_t - z_b$, where z_t and z_b are the heights of the TID upper and lower attachment locations, respectively. Interestingly, similar installation layouts for IVAs with two attachment points were widely adopted for lateral motion control of buildings under wind [33–35] and earthquake loads [31,41] in which the IVAs are attached to between two or more building stories (e.g. by considering floor openings forming a multi-storey internal atrium). Further, the authors of ref. [18] attached an IVA between the nacelle and a lower location inside the WT tower for motion control of a FOWT under wind and wave actions. More importantly, a recent work [42] demonstrated that the TID vibration suppression potential in dynamically excited continuous tapered cantilevered tower-like structures depends significantly on the TID attachment locations, besides the inertance. For this reason, 12 different TID layouts are considered in the numerical part of this work to gauge the influence of the height of the TID attachment locations, their distance L, and the TID inertance b, with properties listed in Table 3. Further, the performance of these TID layouts are compared vis-à-vis the case of a standard TMD installed at the tower top as applied to current industrial WTs [12]. Usually, in practical applications, the secondary mass of the TMD does not exceed 5% of the total structural mass, assumed as a practical upper limit above which the additive dead load of the secondary mass becomes uneconomical to accommodate. In this respect, the secondary mass of the TMD considered as comparison to the TID layouts in Table 3 is taken as $m_d = 35$ t, which is about 5% of the total mass of the adopted benchmark WT system.

2.2. Finite element modelling

The adopted TID-equipped benchmark WT system is modelled in SAP2000 FE software package [37] to support the numerical assessments presented in later sections. The WT tower is modelled using 10 non-prismatic two-node shear-deformable beam elements. These elements feature a linear variation of diameter and thickness following the tower cross section geometric data in [27] (see also Table 2). The WT nacelle is modelled by a 15 m-long beam element with hollow rectangular cross-section, having outer dimensions 7 m × 6 m and 0.1 m thickness. The latter element is assigned a mass equal to the sum of the masses of the nacelle and the hub in Table 1. Further, the blades are explicitly modelled in the FE model of the WT, instead of being represented by an additional lumped mass assigned to the nacelle element, as recommended by recent work on the accuracy of FE models for seismic assessment of WTs [43]. Specifically, the rotor is assumed to be fixed in the position shown in Fig. 1 and each blade is modelled by eight non-prismatic two-node shear-deformable beam elements, following the geometric properties detailed in [27] and the mass property in Table 1. All the structural elements are taken as linearly elastic. A schematic of the developed FE model is shown in Fig. 4a.

The first 12 undamped natural frequencies of the developed FE model along with a qualitative description of the corresponding vibration modes are provided in Table 4, derived by standard modal analysis. They are in a very good agreement with those reported in previous studies (e.g. [39,40]) which adopted the same WT system. This consideration verifies the accuracy of the herein developed FE model. Further, Fig. 4(b) plots the first (dominant) tower mode shape in the fore-aft direction (within x-z plane of the FE model) which is the targeted mode to be suppressed by the TID in Fig. 3. The inherent structural damping of the WT system is introduced to the FE model as modal damping taken equal to 1% for the tower modes and equal to 0.5% for the blade modes.

The TID is implemented in the FE model using the following novel procedure, transferable and generalizable to any other TID modelling

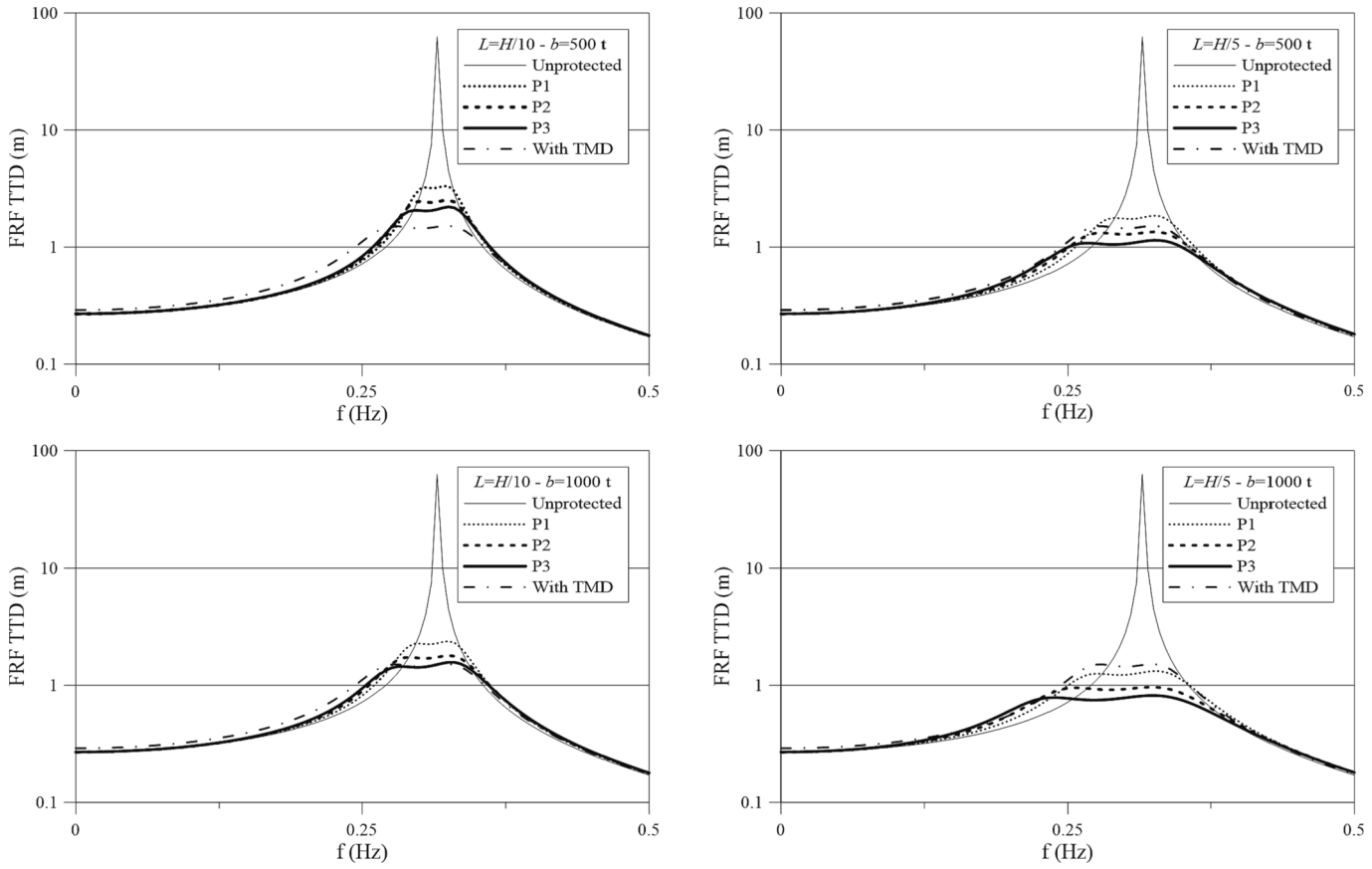

Fig. 6. FRF amplitude for TTD of: (1) wind turbine equipped with TID considering the set of parameters in Table 3, (2) unprotected wind turbine, (3) wind turbine equipped with 35 t TMD at the tower top.

application in standard commercial FE software. The parallel spring-dashpot part of the TID is modelled as a horizontal two-joint link which is a standard element in the library of SAP2000. This link is placed at z_t height with one joint (end) connected to the tower and the other joint to the inerter element. The latter is modelled using a virtual vertical massless rigid beam element of length L as illustrated in Fig. 5. The top end of the virtual inerter beam has a hinge connection at z_t height to the parallel spring-dashpot link element. The bottom end of the virtual inerter beam has a hinge connection at z_b height to an auxiliary horizontal massless rigid beam element which is further connected to the tower (at height z_b) by a rigid connection. The virtual inerter beam is assigned at its geometrical center node a (lumped) mass moment of inertia I_y about the horizonal y-axis to model the inertance property. Based on rotational equilibrium principle, the mass moment of inertia, I_y, corresponding to the inertance b is given as (see also [32])

$$I_y = bL^2 \tag{2}$$

3. Tuning of the tuned inerter damper

The motion control effectiveness of the absorbers in Fig. 2 depends significantly on their tuning, that is, on their stiffness and damping properties, k_d and c_d, respectively, given inertial property (inertance b for the TID and secondary mass m_d for the TMD), host structure properties, and dynamic excitation characteristics. Given the large uncertainty and complexity of the combined wind and earthquake excitation characteristics, it is herein deemed prudent to consider a simple structure-specific type of tuning for the comparative assessment of all the absorbers discussed in the previous section. The adopted tuning is based on the fixed-point theory [44], typically yielding a H_∞ style of optimality as it aims to suppress a single mode shape. Arguably, this is the most widely used tuning for conventional TMDs, providing optimal results for harmonically excited single-degree-of-freedom (SDOF) (see e.g. [45]) and multi-degree-of-freedom (MDOF) [46] host structures. Recently, it was extended to treat the case of TIDs attached to MDOF host structures [47] on adopting a single-mode representation of the structure based on the vibration mode targeted by the absorber. The latter approach is herein applied to the FE model of the WT system in Fig. 4, targeting the 1st tower fore-aft mode, using the following steps.

First, a single-mode representation of the uncontrolled WT system is obtained corresponding to the 1st tower fore-aft mode with natural frequency ω_1 and mode shape vector $\boldsymbol{\varphi_1}$. For TID tuning, the vector $\boldsymbol{\varphi_1}$ is normalized to have a unit relative modal displacement between the two tower locations at which the TID is attached to [47]. For TMD tuning, the vector $\boldsymbol{\varphi_1}$ is normalized to have a unit modal displacement at the tower top, where the TMD is attached to [46]. Then, the generalized modal mass is determined by

$$m_{m1} = \boldsymbol{\varphi_1}^{\mathrm{T}} \mathbf{M} \boldsymbol{\varphi_1} \tag{3}$$

where $\mathbf{M}$ is the mass matrix and the superscript "T" denotes matrix transposition. Next, the TID/TMD frequency is obtained by [45,47]

$$\omega_d = \frac{\omega_1}{1+\mu} \tag{4}$$

where $\mu = b/m_{m1}$ for the TID and $\mu = m_d/m_{m1}$ for the TMD. With the ω_d frequency known from Eq.(4), the TID and TMD stiffness property can be found as $k_d = {\omega_d}^2 b$ and $k_d = {\omega_d}^2 m_d$, respectively. Lastly, the TID/TMD damping ratio can be found by [45,47]

$$\zeta_d = \sqrt{\frac{1}{2}\frac{\mu}{1+\mu}} \tag{5}$$

Table 6
List of selected GMs. M = Magnitude, RSN = record sequence number in the PEER database, T_p = period of the velocity pulse, T_p = duration of the GM.

Earthquake	Station	M	RSN PEER	Tp (s)	duration (s)	Acronyms
Non pulse-like records						
San Fernando 1971	LA - Hollywood Stor FF	6.6	68	–	79.45	SF
Gazli	Karakyr	6.8	126	–	13.50	GA
Tabas 1978	Dayhook	7.4	139	–	21.00	TA
Nahanni 1985	Site 1	6.8	495	–	10.28	NA
Whittier Narrows 1987	LB Orange Ave	6.0	645	–	32.10	WN
Loma Prieta 1989	BRAN	6.9	741	–	25.00	LPB
Loma Prieta 1989	Corralitos	6.9	753	–	39.98	LPC
Cape Mendocino 1992	Cape Mendocino	7.0	825	–	30.00	CMC
Chi Chi 1999	TCU067	7.6	1504	–	90.00	CC1
Chi Chi 1999	TCU084	7.6	1517	–	90.00	CC2
Duzce 1999	Duzce	7.1	1605	–	25.89	DU
Manjil 1990	Abbar	7.4	1633	–	53.52	MA
Parkfield 2004	Parkfield Fault zone 8	6.0	4112	–	21.20	PA
L'aquila 2009	L'Aquila - Aterno - Grilli	6.3	4481	–	40.01	LA
Pulse-like records						
Imperial Valley 06 1979	El Centro Array #6	6.5	181	3.773	39.08	IV1
Imperial Valley 06 1979	El Centro Array #7	6.5	182	4.375	36.85	IV2
Irpinia, 1980	Sturno	6.9	292	3.273	39.34	IR
Superstition Hills 1987	Parachute Test Site	6.5	723	2.394	22.35	SH
Loma Prieta 1989	Saratoga - Aloha Ave	6.9	802	4.571	40.00	LPS
Cape Mendocino 1992	Petrolia	7.0	828	2.996	36.00	CMP
Landers 1992	Lucerne	7.3	879	5.124	48.13	LAN
Northridge-01 1994	Rinaldi Receiving Sta	6.7	1063	1.246	19.90	NOR
Northridge-01 1994	Sylmar - Olive view	6.7	1086	2.436	40.00	NOS
Kobe 1995	Takarazuka	6.9	1119	1.806	40.96	KOR
Kobe 1995	Takatori	6.9	1120	1.554	40.96	KOT
Kocaeli 1999	Izmit	7.5	1165	5.369	30.00	KIZ
Kocaeli 1999	Yarimca	7.5	1176	4.949	35.00	KYA
Denali 2002	TAPS Pump Sta. 10	7.9	2114	3.157	92.10	DE

from which the TID and TMD damping coefficient can be found as $c_d = 2\zeta_d\omega_d b$ and $c_d = 2\zeta_d\omega_d m_d$, respectively. Table 5 reports the stiffness and damping properties obtained using the aforementioned tuning approach for all the TID layouts in Table 3, as well as for a conventional TMD with 35 t secondary mass attached to the tower top.

To gain an insight on the level of first mode suppression achieved by the various absorbers tuned according to Table 5, frequency response functions (FRFs) of the Tower Top Displacement (TTD) of the TID-equipped WT system are plotted in Fig. 6 obtained by applying a unit intensity harmonic ground acceleration along the x direction (fore-aft) of the FE model. The FRFs of the uncontrolled WT and of the TMD-controlled TMD are superposed in all panels of Fig. 6.

Firstly, it is seen in Fig. 6 that both the TID and the TMD produce the typical effect of resonant absorbers tuned by the fixed-point theory. Specifically, in the frequency range where the FRF of the uncontrolled WT exhibits the resonance peak associated with its first modal frequency, the FRFs of all the TID/TMD-equipped WTs exhibit two peaks, associated with two close modal frequencies. As a result of the optimized viscous damping ratio formula in Eq. (5), the two peaks are quite flat and have (almost) the same amplitude [44]. Further, a comparison of the FRFs in Fig. 6 shows that the performance of the TID depends on the parameters b, L and z_t. As expected, for fixed L and z_t, the performance of the TID improves with the inertance b. For fixed b and L, the performance of the TID improves with z_t, i.e., as the TID is installed from position P1 (the lowest) to position P3 (the highest). Moreover, for fixed b and z_t, the performance improves with the increase of the distance L. These trends confirm previous findings in the literature for beam-like cantilever tapered structures equipped with TID [42], attributed to the fact that, in the first mode shape vector of the uncontrolled WT, attachment locations at a larger distance and/or at higher elevations are characterized by a larger difference of modal displacements (see mode shape of the tower in Fig. 4b), which improves the engagement of the TID. At the same time, it is noted that the TMD achieves better performance in the vicinity of ω_1, compared to at least all TID layouts with $L = H/10$. However, TID outperforms the TMD for most of the lower frequencies range. In every case, the actual performance of the TID/TMD-equipped WT system will heavily depend on the wind and earthquake excitation characteristics and, thus, performance assessment in time-domain for various recorded earthquake excitations and at different wind speeds is required. This is addressed in detail in the following Section.

4. Performance assessment of TID-equipped benchmark WT

In this Section, pertinent numerical results are reported and discussed, aiming to assess the efficiency of different TID layouts and of a conventional TMD in reducing the dynamic response of the adopted WT benchmark system under strong earthquake ground motions (GMs). As earthquakes may obviously occur during the operation of the WT, the thrust force due to wind loads is also considered (e.g. [43,48]). The presentation begins by describing the wind action representation in the SAP2000 FE model of the WT system.

4.1. Wind action representation

Consistently with the orientation of the rotor in the FE model, the thrust force acts in the x (fore-aft) direction. In agreement with several studies in the literature, the thrust force is modelled as a point load applied to the rotor center [49–51]. This simplifying assumption is reasonable in the context of this study, whose focus is the dynamics of the support tower and the reduction of its vibrations by the TID/TMD. Specifically, the thrust force is given as

$$F_{Th}(t) = \frac{1}{2}\rho_{air} C_t A_{rotor} u^2(t) \tag{6}$$

where ρ_{air} is the air density, A_{rotor} is the rotor disc area, C_t is the thrust coefficient and $u(t)$ is the instantaneous wind velocity. The thrust coefficient C_t is obtained by fitting Eq.(6) to data in Fig. 9.1 of ref. [27]. Moreover, to account for the aerodynamic damping associated by the interaction between wind and rotor, an additional 4% modal damping is attributed to the tower modes, in agreement with previous studies [52–53].

The time histories of wind speed in Eq.(6) are generated using the well-established spectral representation method for power spectrum compatible simulation [54]. For this simulation, the Kaimal turbulence model is adopted in accordance with the IEC prescriptions [55], represented by the power spectrum in the domain of frequencies f

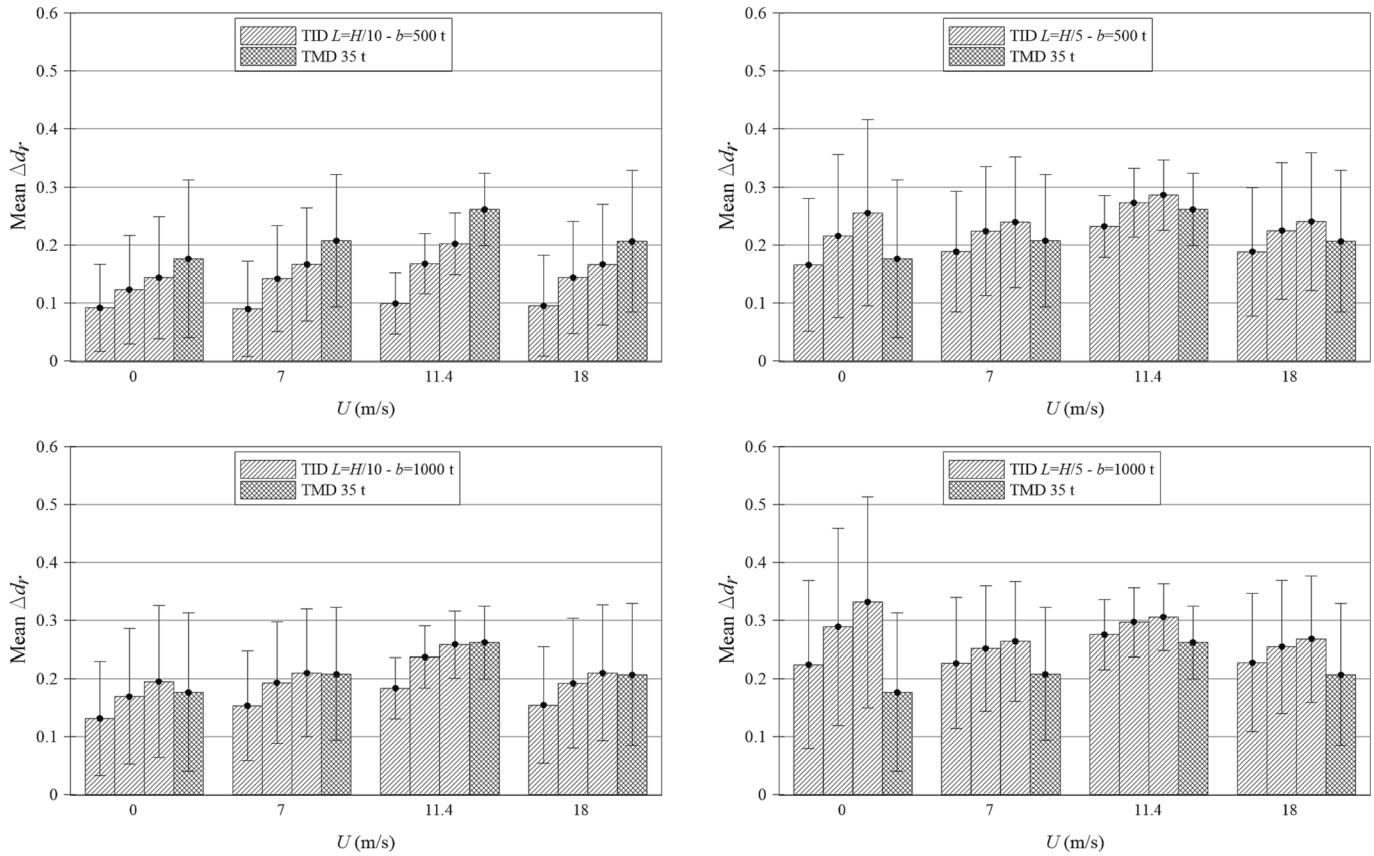

Fig. 7. Variations of maximum TTD for $L = H/10$ (left) and $L = H/5$ (right), for $b = 500$ t (top) and $b = 1000$ t (bottom) and different wind speeds, averaged over all GMs. Each group of four bar plots contains, for a given wind speed, the values for three positions of the TID along the tower and for the TMD; from the left to the right: TID in P1, P2, P3 and TMD. Thin whiskers indicate the deviation from the mean, calculated as twice the standard deviation of the variations obtained for the GMs.

$$S(f) = \frac{4\sigma_k^2 L_k/U}{(1 + 6fL_k/U)^{5/3}} \tag{7}$$

where U is the mean wind speed and $L_k = 340.2$ m is the turbulence length in the longitudinal direction considered in this study. Further, in Eq. (7) σ_k is the standard deviation of the turbulence, related to the turbulence intensity I_{ref} that, in turn, depends on the mean wind speed U. In particular, the IEC category B turbulence model is adopted to compute the standard deviation σ_k, as:

$$\sigma_k = I_{ref}(0.75U + 5.6) \tag{8}$$

where I_{ref} is taken equal to 0.14 [55].

Four mean wind speeds are selected for the numerical analyses: $U = 0{-}7{-}11.4{-}18$ m/s. For $U = 0$ m/s, there is no wind and the turbine is parked. The wind speeds $U = 7{-}11.4{-}18$ m/s are below, equal and above the rated wind speed $U = 11.4$ m/s, respectively. At the rated wind speed, i.e., the minimum wind speed at which the turbine operates at the rated power, the highest value of the thrust force occurs.

Notice that there exist alternative and more refined approaches to model the operational thrust force acting on FE models of wind turbines as, e.g., the approach in ref. [56] where time histories of the thrust force are generated by FAST. However, modelling the thrust force by Eq. (6) may be considered as acceptable in the context of this study, whose focus is on the protection of the wind turbine from earthquake-induced vibrations. Moreover, other studies in the literature made use of approximate analytical expressions for the operational thrust force, see e.g. ref. [57,58].

4.2. Earthquake action representation

Earthquake action is represented by recorded acceleration GMs at the tower base in the x (fore-aft) direction of the FE model. A set of 28 GMs are selected from the PEER database [59]: 14 pulse-like GMs with average pulse period of 3.35 s which is close to the natural period of the 1st tower mode (3.16 s) and 14 non-pulse-like records. In all cases, the first horizontal GM component from each recording station is chosen. The complete list of the GMs is reported in Table 6. The need to distinguish between pulse-like and non-pulse-like GMs stems from recent works demonstrating that WT towers are particularly susceptible to pulse-like GMs, especially to those with pulse-period close to the tower natural periods [48,60].

To calculate the response under combined earthquake and wind loads, it is assumed that each GM starts at $T_0 \geq 50$ s into the simulation, so that the earthquake occurs as the system response to thrust force has reached a steady state.

4.3. Performance metrics

Time-domain numerical analyses are carried out in SAP2000 using the Newmark algorithm for direct integration of the equations of motion on FE models of the uncontrolled WT and the TID/TMD-equipped WT for the tuning parameters in Table 3. Performance is gauged in terms of the maximum TTD, the maximum tower top acceleration (TTA), the maximum tower base bending moment (TBBM), the maximum tower base shear (TBS), and the maximum TID/TMD stroke $|x_1 - x_d|$ in Fig. 2. These quantities are evaluated for all the GMs in Table 6 and the four selected mean wind speeds $U = 0{-}7{-}11.4{-}18$ m/s, for the 12 layouts of

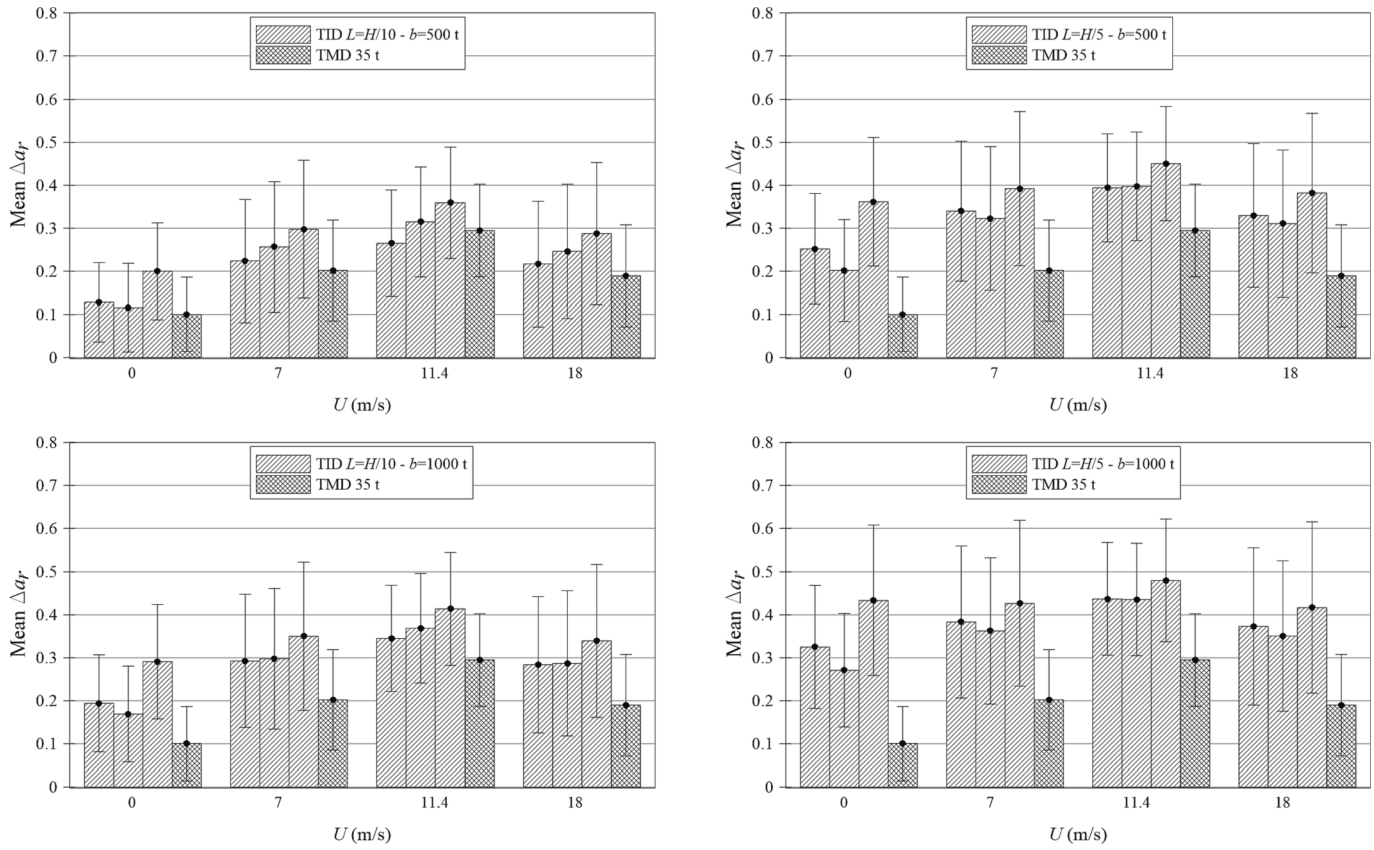

Fig. 8. Variations of maximum TTA for $L = H/10$ (left) and $L = H/5$ (right), for $b = 500$ t (top) and $b = 1000$ t (bottom) and different mean wind speeds, averaged over all GMs. Each group of four bar plots contains, for a given wind speed, the values for three positions of the TID along the tower and for the TMD; from the left to the right: TID in P1, P2, P3 and TMD. Thin whiskers indicate the deviation from the mean, calculated as twice the standard deviation of the variations obtained for the GMs.

the TID and the 35 t TMD in Table 5 and for the unprotected wind turbine. In the simulations under combined earthquake and wind loads, the maxima of the response are evaluated for $t > 50$ s.

The performances of the TID and the TMD are assessed by comparing the maximum response of the controlled WT system versus the maximum response of the uncontrolled WT system. This is accomplished by using the following performance metrics

$$\begin{aligned} \Delta d_r &= \frac{d_{nd} - d_{wd}}{d_{nd}}; \\ \Delta a_r &= \frac{a_{nd} - a_{wd}}{a_{nd}}; \\ \Delta M_r &= \frac{M_{nd} - M_{wd}}{M_{nd}}; \\ \Delta S_r &= \frac{S_{nd} - S_{wd}}{S_{nd}} \end{aligned} \tag{9}$$

where d_{nd}, a_{nd}, M_{nd} and S_{nd} are the maximum TTD, TTA, TBBM, and TBS of the uncontrolled WT system, while d_{wd}, a_{wd}, M_{wd} and S_{wd} are the same quantities, respectively, for the controlled WT system. Therefore, a positive performance metric value in Eq. (9) means that the absorber reduces the corresponding maximum response quantity, while a negative performance metric value means that the presence of the absorber is detrimental.

4.4. Numerical results and discussion for time instant of earthquake occurrence $T_o = 50$ s

For the ease of reading, the variations of maxima TTD, TTA, TBBM and TBS are illustrated in separate Figures. Each Figure includes four sub-Figures corresponding to the four possible combinations of L, i.e., the distance between the points at which the TID is mounted and b, i.e., the inertance. In the sub-Figures, the results are grouped by mean wind speed $U = 0{-}7{-}11.4{-}18$ m/s; each group includes from left to right the results for the three selected positions of the TID, i.e., P1, P2, P3 in Table 3, while the fourth result on the right is that for the TMD.

Fig. 7 shows the variations of maximum TTD, in terms of mean and deviation from the mean. The mean is calculated across the 28 GMs and is indicated by the bar plots. The deviation from the mean is twice the standard deviation of the variations obtained for the 28 GMs and is indicated by the thin whiskers extending above and below the mean values (bar plots). Clearly, the longer the whisker is, the higher the variability of the responses is across the 28 GMs.

First, attention is focused on the mean variations in Fig. 7. It is seen that the results for the wind turbine with TID mirror the FRFs shown in Fig. 6, obtained under a unit harmonic ground acceleration. Indeed, the capability of the TID in reducing the maximum TTD increases with the inertance b. Moreover, as the TID moves towards the tower top, the efficiency increases. This behaviour may be attributed to the fact that the first mode shape, which is targeted by the TID, features a monotonically increasing gradient of horizontal displacement from the tower base to the tower top. Therefore, the TID is better activated when mounted closer to the tower top (z_t for position P3 is higher than z_t for positions P2 and P1, see Table 3 and Fig. 3). Furthermore, the performances improve with the distance L between the points at which the TID is mounted along the tower. These improvements relate to the fact that, in the first mode shape targeted by the TID, a larger distance L implies a larger relative motion between the terminals of the TID, i.e., the TID is activated more for larger distance L [42]. Additional comments concern the comparison among the results for different wind speeds. For $L = H/5$

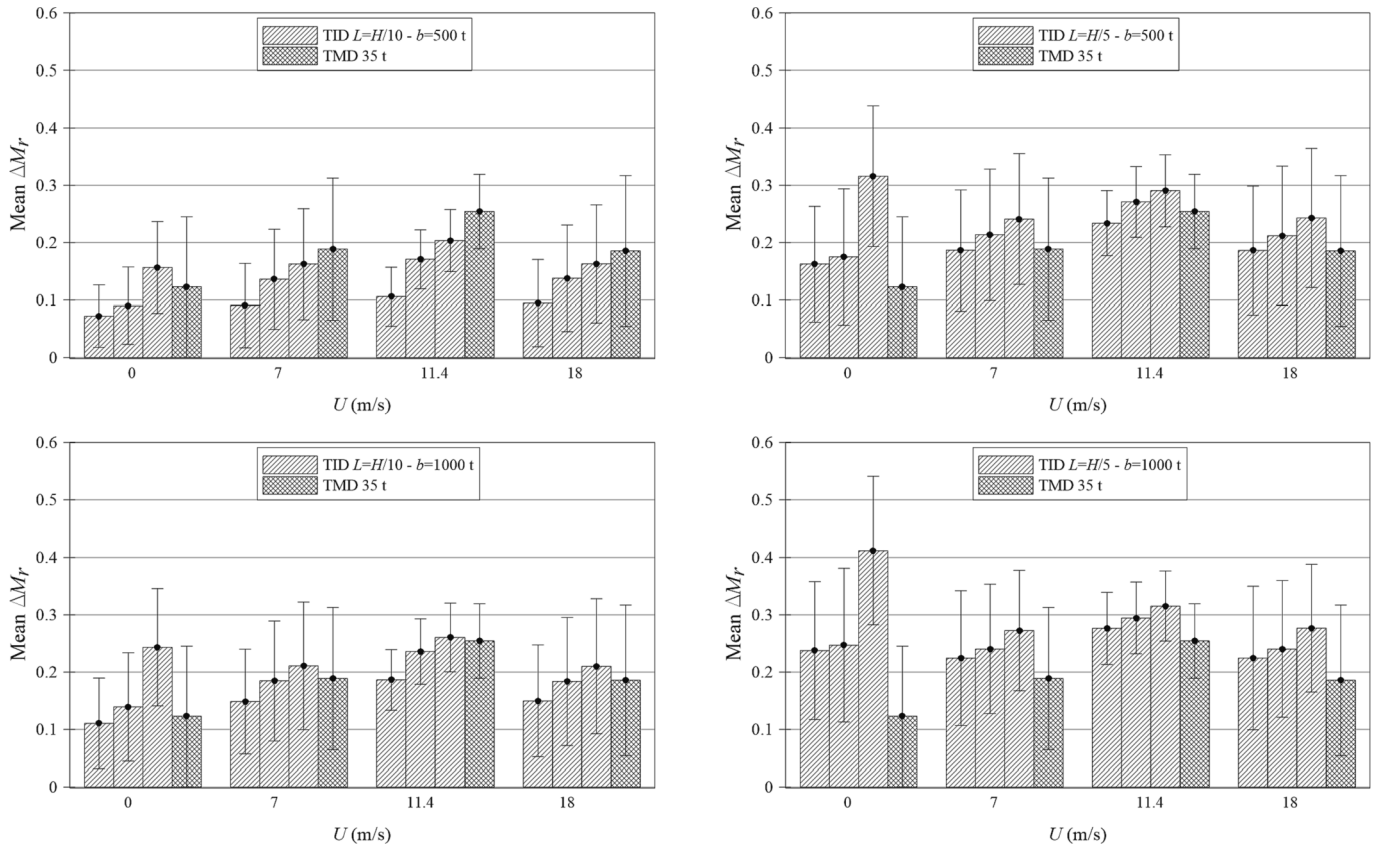

Fig. 9. Variations of maximum TBBM for $L = H/10$ (left) and $L = H/5$ (right), for $b = 500$ t (top) and $b = 1000$ t (bottom) and different mean wind speeds, averaged over all GMs. Each group of four bar plots contains, for a given wind speed, the values for three positions of the TID along the tower and for the TMD; from the left to the right: TID in P1, P2, P3 and TMD. Thin whiskers indicate the deviation from the mean, calculated as twice the standard deviation of the variations obtained for the GMs.

and $b = 1000$ t, the best performances of the TID are obtained in absence of wind ($U = 0$ m/s), while for the other layouts the TID performs better at the rated wind speed $U = 11.4$ m/s. More importantly, for any wind speed considered including the no wind case, the same set of parameters in Table 3 provides the best performances of the TID. This is the set $L = H/5$, $b = 1000$ t and position P3, for which the mean reduction of the maximum TTD attains almost 35% in absence of wind ($U = 0$ m/s) and about 30% for $U = 11.4$ m/s. This observation confirms the potential of the TID for seismic protection of the wind turbine.

Further, consider the deviations from the mean in Fig. 7. The results demonstrate that the TID is never detrimental to the response of the wind turbine. Indeed, the low end of the whiskers never goes below the zero. This observation establishes the robustness of the TID performance to the variability of GMs, considering that the 28 GMs in Table 6 have very different properties.

For completeness, consider the results reported in Fig. 7 for the wind turbine with TMD. For all the wind speeds, the efficiency of the TMD is slightly higher than those of the TID obtained for $L = H/10$ and $b = 500$ t, comparable with those obtained for $L = H/10$ and $b = 1000$ t and significantly lower than those obtained for $L = H/5$, especially for $b = 1000$ t and in absence of wind ($U = 0$ m/s). Regarding the deviation from the mean in Fig. 7, it is apparent that the TID behaves better than the TMD: indeed, the upper end of whiskers for TID attains values even above the 50%, which is not the case of the TMD. From this comparison, it is seen that the TID outperforms the TMD for sufficiently high values of inertance (which is readily scalable in practice and practically independent of the device weight) and/or distance L between the two TID attachment locations.

Fig. 8 reports the variations of maximum TTA. The results for the wind turbine with TID are consistent with those in Fig. 7, as the mean reduction of the maximum TTA improves with the inertance b and with the distance L. As for the position along the tower, the efficiency of the TID generally increases as the TID moves towards the tower top, although, for $L = H/5$ with all mean wind speeds and for $L = H/10$ in absence of wind, the TID is slightly less efficient in the position P2 than in the position P1. As for the results for different wind speeds, the largest mean reductions of maximum TTA occur for $U = 11.4$ m/s, while the lowest mean reductions occur in absence of wind ($U = 0$ m/s). Again, the set of parameters in Table 3 providing the best efficiency of the TID is $L = H/5$, $b = 1000$ t and position P3, for which the mean reduction of the maximum TTA attains almost 50% for $U = 11.4$ m/s and 45% for $U = 0$ m/s. Recognize that reducing the maximum TTA is an important target of design, meaning that the inertial forces acting on the nacelle and the components within it (drivetrain, gearbox, generator, yaw system) are significantly reduced [2]. Comparing the results for the wind turbine with TID to those for the wind turbine with TMD shows that, in terms of TTA, the TID performs much better than the TMD across the board. Indeed, with the TMD, the mean reduction of the maximum TTA is about 30% for $U = 11.4$ m/s and about 10% for $U = 0$ m/s. Therefore, it is concluded that the inertial forces acting on the nacelle and the components within the nacelle are more efficiently reduced by a TID than by a TMD. This aspect may be attributed to the fact that the TID achieves wideband damping effect which suppresses higher modes, beyond the targeted/resonant one, relevant to acceleration-related dynamic response [34,41]. Further comments on the results in Fig. 8 concern the deviation from the mean: it is apparent that the TID acceleration suppression improvement is more robust than the TMD to the GM variability, while for some GMs improvements of more than 50% are noted (i.e., upper end of whiskers are above 0.5) for the TID layouts with $L = H/5$, $b = 1000$ t.

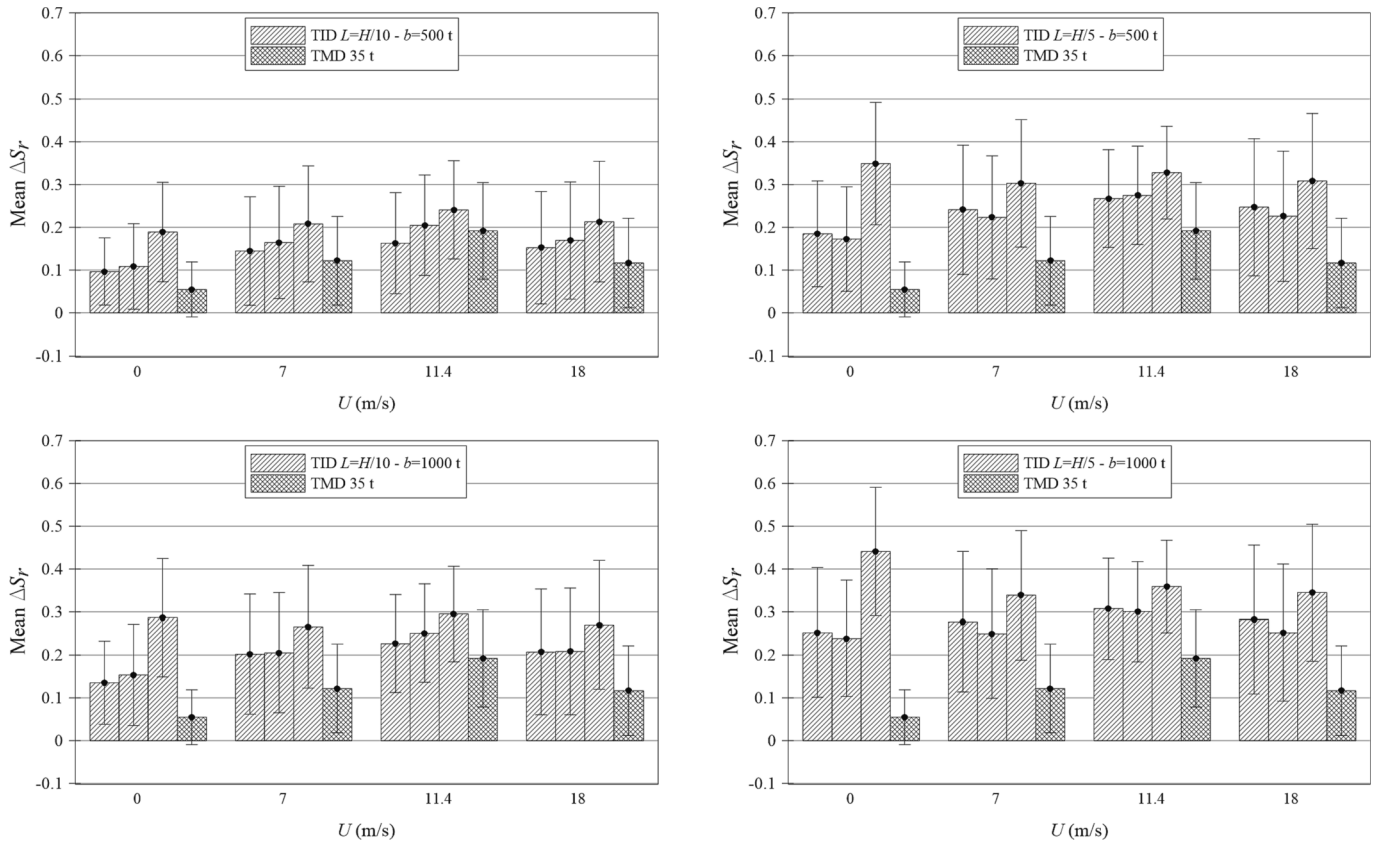

Fig. 10. Variations of maximum TBS for $L = H/10$ (left) and $L = H/5$ (right), for $b = 500$ t (top) and $b = 1000$ t (bottom) and different mean wind speeds, averaged over all GMs. Each group of four bar plots contains, for a given wind speed, the values for three positions of the TID along the tower and for the TMD; from the left to the right: TID in P1, P2, P3 and TMD. Thin whiskers indicate the deviation from the mean, calculated as twice the standard deviation of the variations obtained for the GMs.

Thereafter, attention moves to the effectiveness of the TID in reducing the stress at the tower base. Fig. 9 shows the variations of maximum TBBM. The reported data exhibit the same general trends as those observed for the maximum TTD in Fig. 7 and the maximum TTA in Fig. 8: the mean reduction of the TBBM increases with the inertance b, with the distance L and as the TID moves towards the tower top. Regarding the results for different wind speeds, the mean reductions of maximum TBBM are better in absence of wind ($U = 0$ m/s) for $L = H/5$, while for $L = H/10$ the TID performs slightly better for $U = 11.4$ m/s. As before, the set of parameters $L = H/5$, $b = 1000$ t and position P3 is the set providing the best performances of the TID overall, i.e., both in absence of wind ($U = 0$ m/s) and for any wind speed $U = 0{-}7{-}11.4{-}18$ m/s. Specifically, for the above set of parameters, the mean reduction of the maximum TBBM is more than 30% for $U = 11.4$ m/s and more than 40% in absence of wind ($U = 0$ m/s). Additionally, Fig. 10 illustrates the variations of maximum TBS. The results exhibit the same trend observed for the maxima TTD, TTA and TBBM with the inertance b, the distance L and the position along the tower. Concerning the results for different wind speeds, in this case the mean reduction is better for $U = 11.4$ m/s when $L = H/10$, while it is better for $U = 0$ m/s when $L = H/5$. In every case, the best performance of the TID across all wind speeds is always obtained for the set of parameters $L = H/5$, $b = 1000$ t and position P3, with mean reductions above 40%. For this set of parameters, therefore, the mean reductions of maximum TBBM in Fig. 9 and maximum TBS in Fig. 10 demonstrate that the TID may ensure a significant protection of the wind turbine under strong earthquake motions. As for the wind turbine with TMD, Fig. 9 and Fig. 10 show that the TMD causes mean variations of the maxima TBBM and TBS significantly smaller than the correspondent quantities obtained with the TID. This is especially evident in absence of wind ($U = 0$ m/s). On the other hand, the deviation from the mean suggests that the performance of the TID may attain values above the 50%. This is not the case of the wind turbine with the TMD.

Next, Fig. 11 shows the maximum stroke for all the set of parameters in Table 3 and for the 35 t TMD. Each histogram indicates the maximum stroke over those obtained for the twenty-eight GMs. Inspection of Fig. 11 reveals that, for fixed inertance b, larger strokes occur for larger values of L and as the TID moves towards the top. As the stroke may be taken as a measure of the activation of the TID, these results are consistent with mean reductions of the maximum TTD shown in Fig. 7, which improve with larger values of L and as the TID moves towards the top. On the other hand, the maximum stroke decreases as the inertance b increases. The largest stroke values always occur for $U = 0$ m/s. The overall maximum stroke is about 0.45 m, which makes suitable the choice of placing the TID within the tower, as shown in Fig. 3. In contrast, the overall maximum stroke of the TMD may attain values above 1.8 m, which results in higher device cost and increases clearance demands in the nacelle/tower.

Finally, time histories of the TTD are shown in Fig. 12 and Fig. 13, for all the considered mean wind speeds U and three different systems: the unprotected wind turbine, the wind turbine equipped with a 35 t TMD and the wind turbine equipped with a 1000 t TID, for $L = H/5$ and position P3 (layout 12 of Table 3). Specifically, two GMs are taken as examples from the twenty-eight GMs in Table 6: the non pulse-like "CC2" in Fig. 12 and the pulse-like "IR" in Fig. 13. Notice that the first 50 s of the time histories are not shown, as every GM starts 50 s into the simulation to ensure that the thrust force attains a steady state; further, 20 more seconds are discarded in Fig. 12, because for GM "CC2" the ground accelerations are negligible in the first 20 s.

In Fig. 12, the maximum TTD is significantly reduced for all the

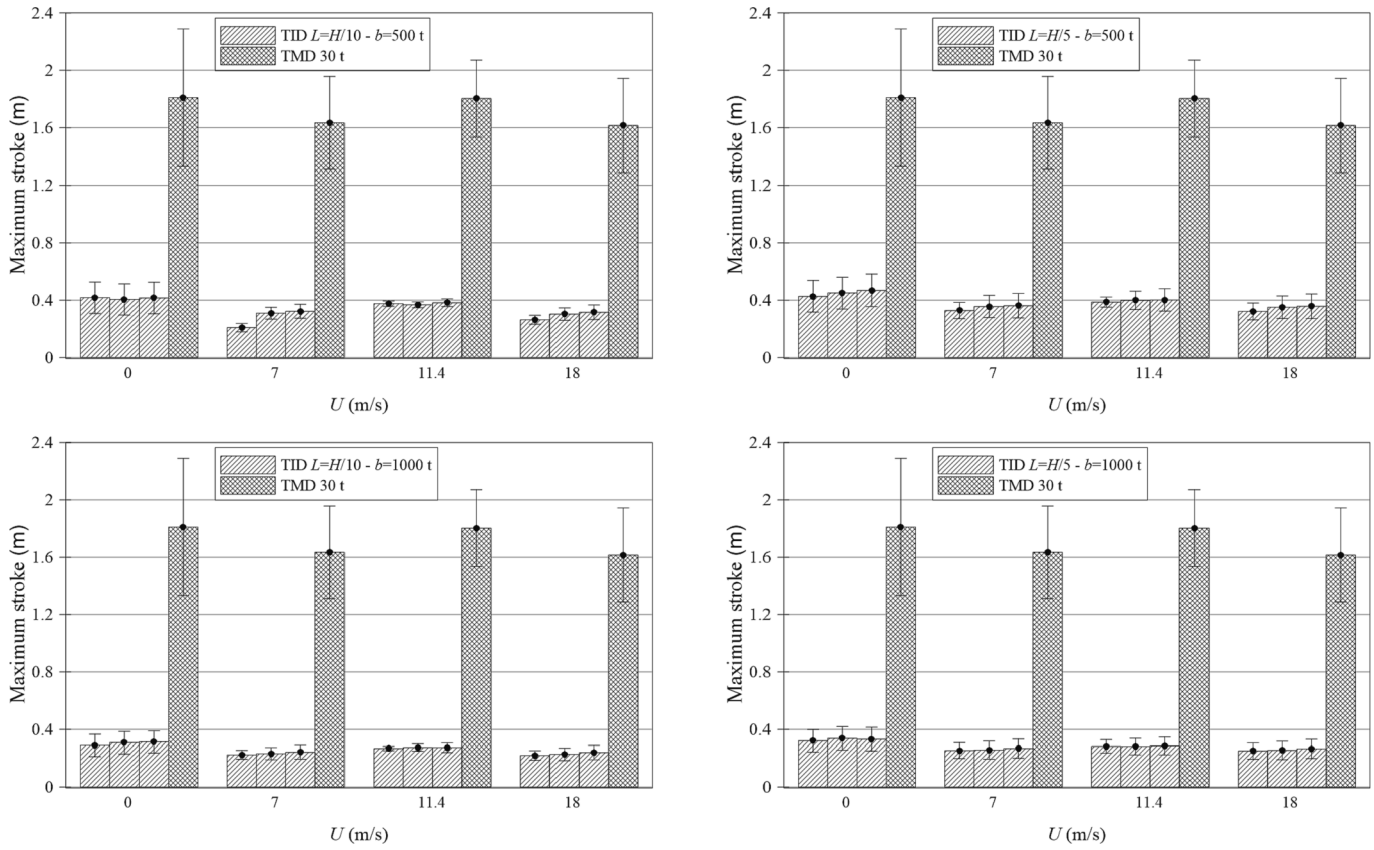

Fig. 11. Maximum spring-dashpot (absolute value of) stroke for $L = H/10$ (left) and $L = H/5$ (right), for $b = 500$ t (top) and $b = 1000$ t (bottom) and different mean wind speed. Each bar plot is the maximum over all GMs. Each group of four bar plots contains, for a given wind speed, the values for three positions of the TID along the tower and for the TMD; from the left to the right: TID in P1, P2, P3 and TMD. Thin whiskers indicate the deviation from the mean, calculated as twice the standard deviation of the variations obtained for the GMs.

considered mean wind speeds. For $U = 0$ m/s, the maximum TTD is equal to 1.08 m for the unprotected wind turbine and 0.59 m for the wind turbine equipped with the TID, meaning that the maximum TTD reduction is about 45%. For $U = 7$–11.4–18 m/s, the reductions of the maximum TTD are in the range 35–42%. Moreover, for all the considered mean wind speeds, not only the maximum TTD is significantly reduced, but also the various peaks of the time histories, often by more than 45%. Notably, the system equipped with the TID behaves much better than the system equipped with the 35 t TMD.

The results in Fig. 13 are qualitatively similar to those in Fig. 12. For $U = 0$ m/s, the maximum TTD is equal to 0.59 m for the unprotected wind turbine and 0.26 m for the wind turbine equipped with the TID, i.e., in this case the reduction of the maximum TTD equal to the remarkable value of about 56%. In presence of wind, i.e., for $U = 7$–11.4–18 m/s, the reductions of the maximum TTD are in the range 38–43%. Again, not only the maximum TTD is significantly reduced but also the various peaks of the time histories, and the performance of the system equipped with the TID are significantly better than those obtained with the 35 t TMD.

The comments above hold also for the time histories of the TTA, TBBM and TBS, and pertinent Figures are not reported for brevity. These results confirm the effectiveness of the TID, which can be considered as a valuable device to protect wind turbines from earthquake induced vibrations.

4.5. Influence of time instant of earthquake occurrence T_0

In the previous section, the time instant of the earthquake occurrence, T_0, was taken constant and equal to $T_0 = 50$ s. In this section, additional numerical data are presented to assess the influence of varying T_0 on the peak values of TTD, TTA, TBBM, TBS and TID stroke. Specifically, results obtained from 6 different values of T_0 ranging from 50 s to 75 s at a step of 5 s.

Fig. 14 shows the variations of maximum TTD for $L = H/5$ and $b = 1000$ t, i.e., for layouts 10, 11 and 12 in Table 3 and for the 35 t TMD, for each of the 6 considered values of T_0. It is apparent that changing the time instant of earthquake occurrence T_0 does not change general trends and conclusions drawn in the previous section on the effectiveness of the TID. Indeed, it is observed that the best performance of the TID is always obtained for the set of parameters $L = H/5$, $b = 1000$ t and position P3, regardless of T_0. Further, the best performance of the TID in terms of mean reduction of maximum TTD is obtained for $U = 11.4$ m/s for all T_0 values considered. Still, it is observed that the mean reduction of maximum TTD for the set of parameters $L = H/5$, $b = 1000$ t and position P3 and for $U = 11.4$ m/s varies in the range 31%–44%. Although such variation with T_0 is certainly not negligible, it is most important to note, from the design viewpoint, that an improved performance of the TID-equipped structure by at least 30% is achieved across all T_0 values. Moreover, the TID outperforms the TMD for all considered T_0 values.

Notably, similar trends with T_0 apply for all the other performance indices previously discussed. For illustration, mean reductions of maxima TTD, TTA, TBBM, TBS and TID stroke are plotted in Fig. 15 as a function of T_0 for the set of parameters $L = H/5$, $b = 1000$ t and position P3 and for three different mean wind speeds. It is found that the mean reductions of maxima TTD, TBBM, TBS exhibit the same variation trend with T_0, within a range of about 10–12% for the considered values of T_0. Meanwhile, the mean reduction of maximum TTA and maximum stroke are less influenced by T_0. Specifically, the mean reduction of maximum TTA varies by less than 4%, while the maximum stroke varies by less than 0.05 m, for all of the considered mean wind speeds. These results

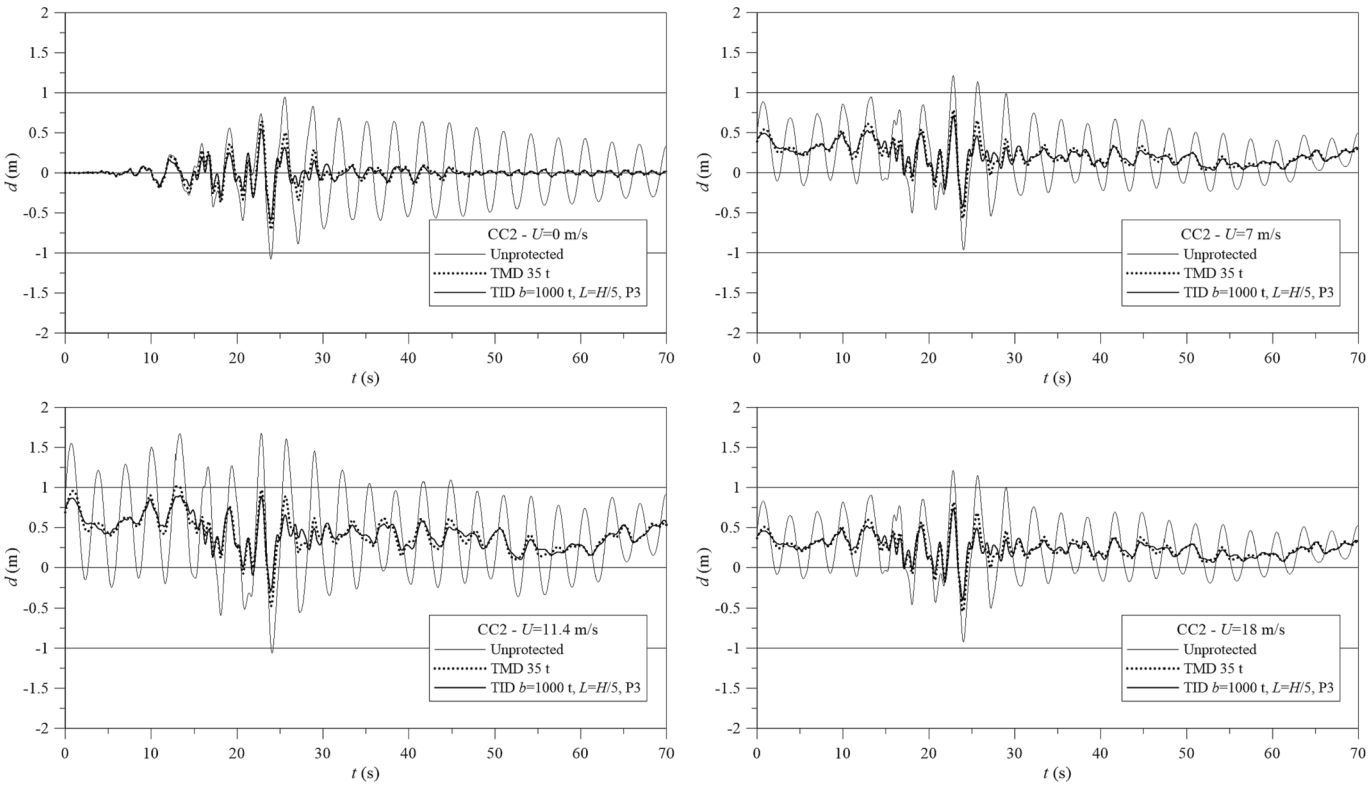

Fig. 12. Time histories of TTD under the GM "CC2" in Table 6, for all the considered wind speeds and three systems: the unprotected wind turbine, the wind turbine equipped with a 35 t TMD and the wind turbine equipped with a 1000 t TID, for $L = H/5$ and position P3 (layout 12 of Table 3).

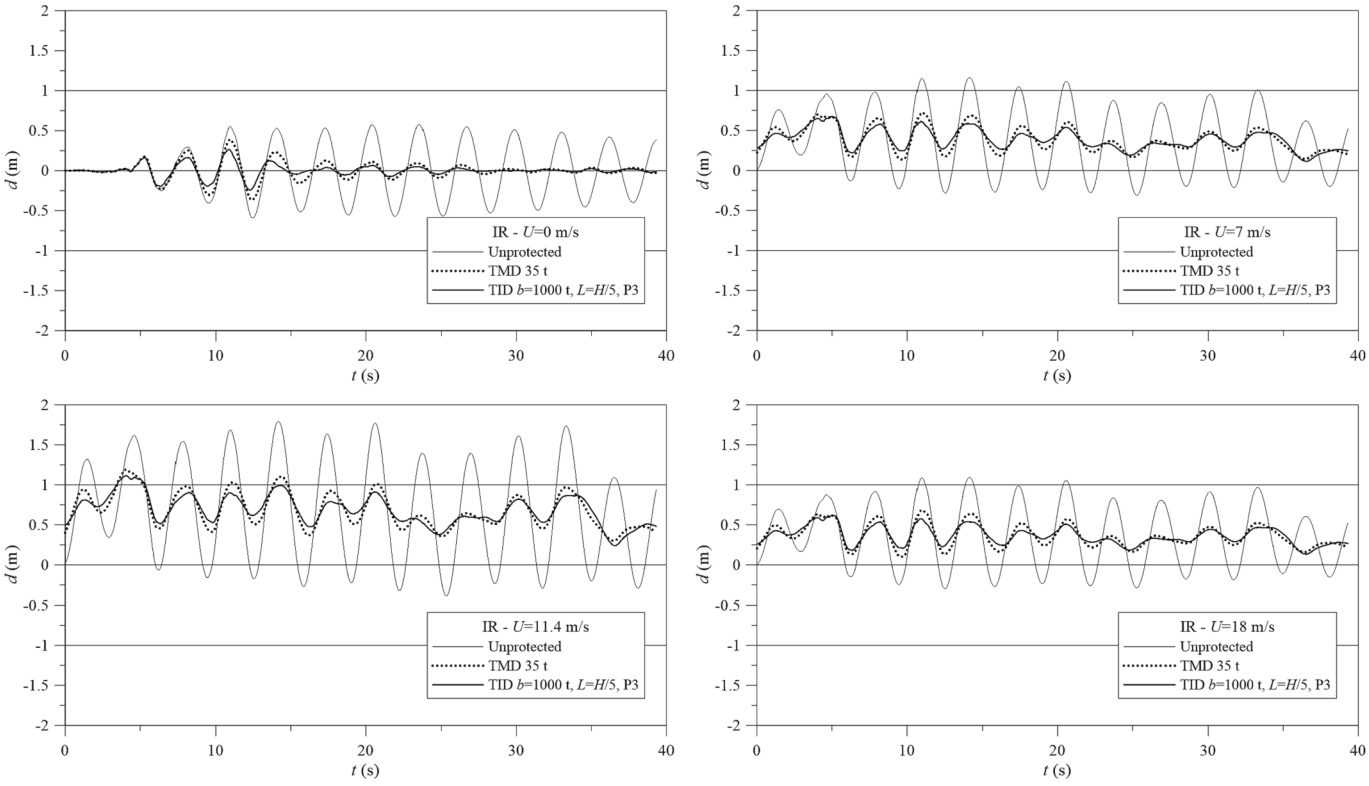

Fig. 13. Time histories of TTD under the GM "IR" in Table 6, for all the considered mean wind speeds and three systems: the unprotected wind turbine, the wind turbine equipped with a 35 t TMD and the wind turbine equipped with a 1000 t TID, for $L = H/5$ and position P3 (layout 12 of Table 3).

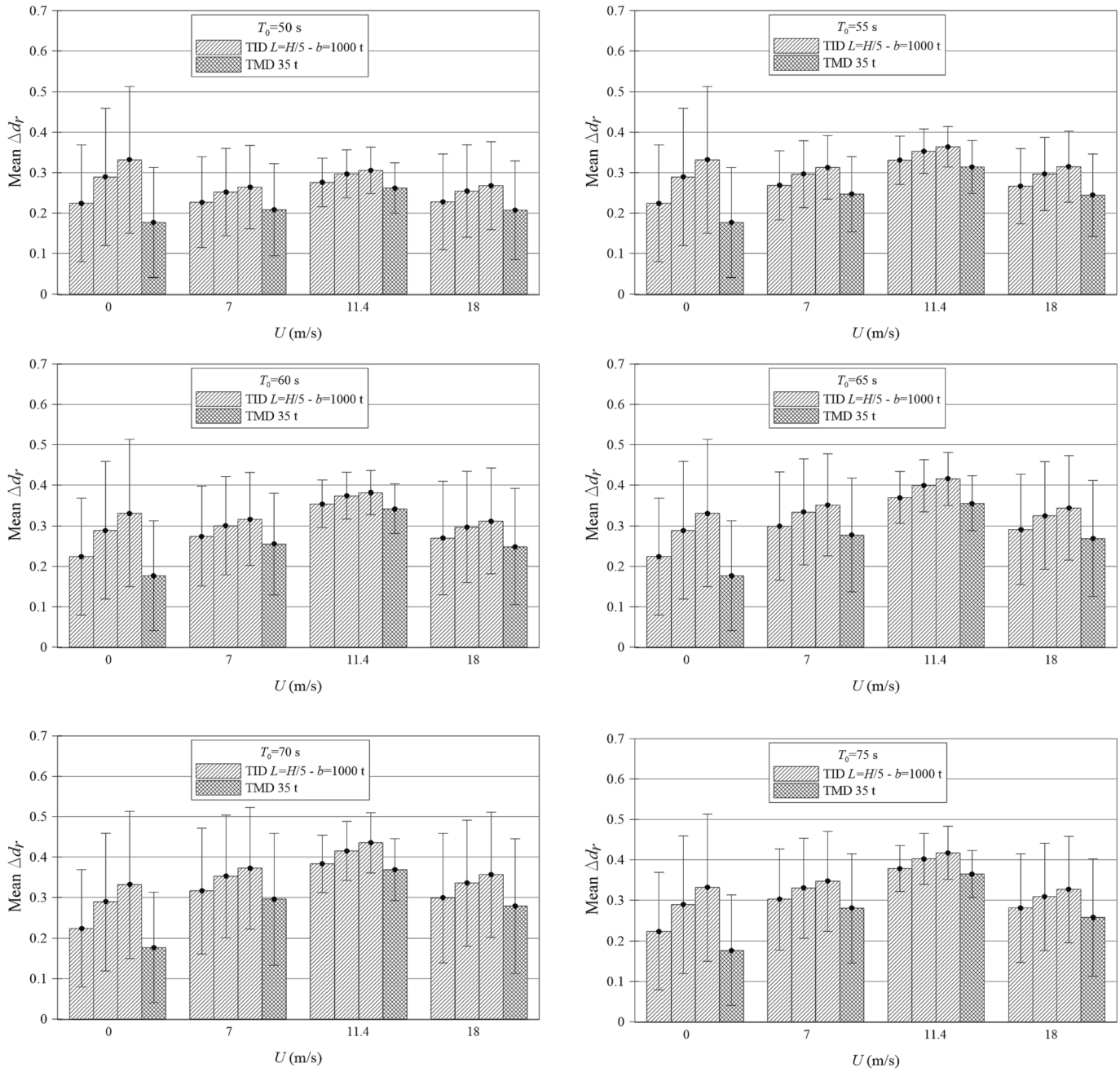

Fig. 14. Variations of maximum TTD for $L = H/5$ and $b = 1000$ t and different wind speeds, averaged over all GMs. Each subfigure pertains to a different time instant of earthquake occurrence T_0. Each group of four bar plots contains, for a given wind speed, the values for three positions of the TID along the tower and for the TMD; from the left to the right: TID in P1, P2, P3 and TMD. Thin whiskers indicate the deviation from the mean, calculated as twice the standard deviation of the variations obtained for the GMs.

confirm the robustness of the proposed TID concept with respect to the mean wind speed and time instant of earthquake occurrence.

5. Concluding remarks

The effectiveness of the tuned inerter damper (TID) for mitigating the vibration response of land-based wind turbines (WTs) under earthquake excitations was established numerically. This was achieved by migrating the TID concept with non-grounded inerter and its tuning from multi-storey building structure applications to the case of WT towers, for the first time in the literature. Numerical work was supported by a finite element (FE) model of a widely studied industrial benchmark WT system developed in SAP2000 commercial software, including an ad hoc and readily implementable modelling approach of the TID. Using a fixed-point theory-based calibration procedure to tune the TID, the numerical analyses were conducted, including a preliminary assessment in the frequency domain under unit harmonic ground acceleration and comprehensive time-domain simulations for different TID layouts, under combinations of 28 pulse-like and non-pulse-like recorded ground motions (GMs) and 4 mean wind speeds. The results showed that the TID vibration suppression effectiveness improves by increasing the TID inertance and/or the distance of the two TID attachment locations along the WT tower. Further, an improvement of the TID performances was also noted by installing the TID closer to the tower top. Among the considered sets of geometric/mechanical parameters of the TID, a specific set is identified as that providing considerable reductions of the

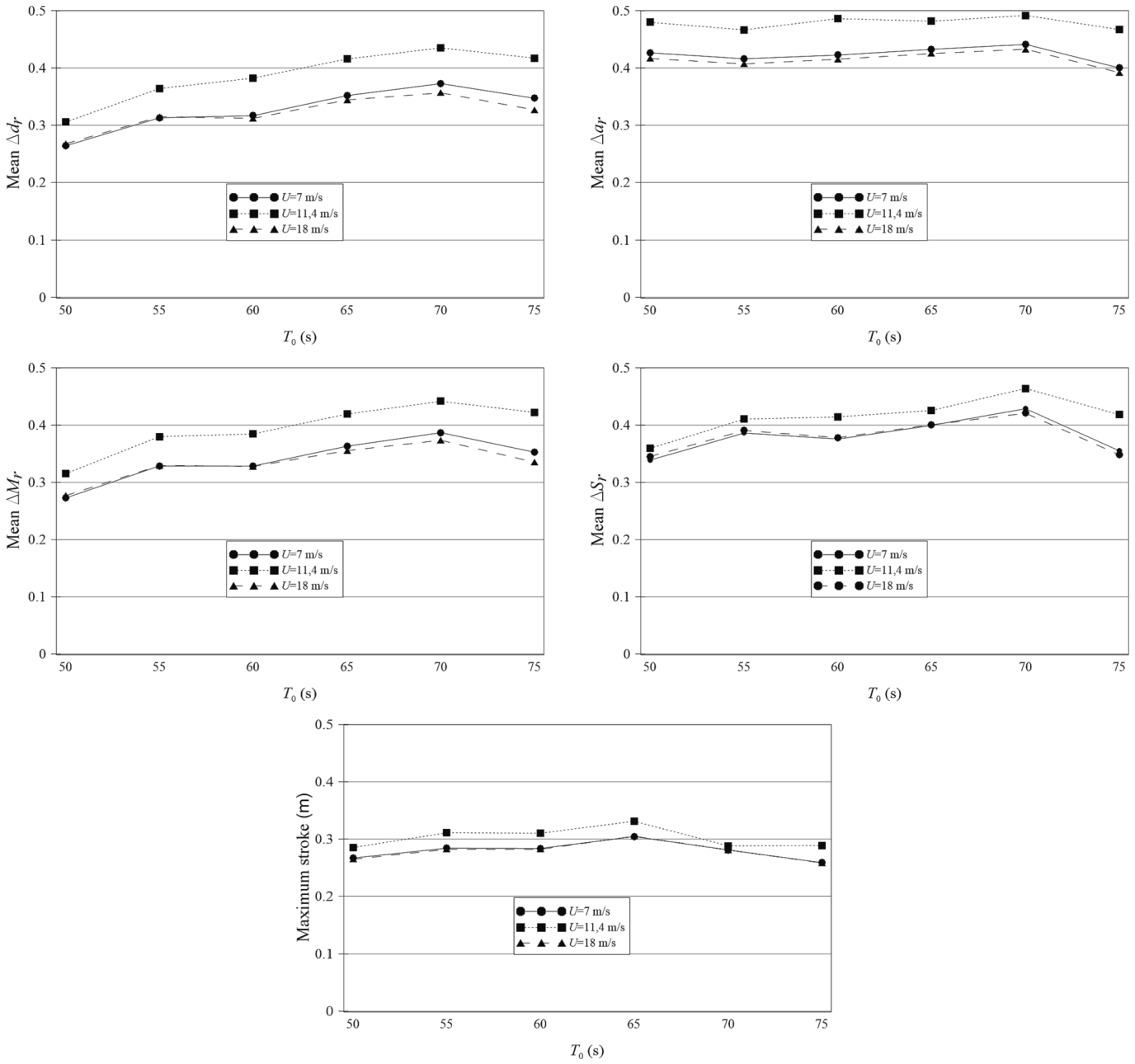

Fig. 15. Variations of maxima TTD, TTA, TBBM, TBS and stroke with time instant of earthquake occurrence T_0 for $L = H/5$, $b = 1000$ t and position P3 and different wind speeds, averaged over all GMs.

response at the tower top and at the tower base, for any of the selected wind speeds and in absence of wind. This is a remarkable outcome of the study, which facilitates practical structure-specific TID design and placement. Finally, the results demonstrate that using a TID brings significant advantages compared to applying a standard TMD at the tower top. Specifically, the TID consistently improves the WT dynamic response for all the different combinations of GM excitations and wind speeds more than the TMD. Moreover, the TID was shown to undergo strokes suitable for the space available within the tower. These observations corroborate the advantages of the herein proposed TID configuration for WT tower protection over the currently used TMD.

To this end, the overarching conclusions of this study are summarized as follows:

- The TID motion control capability always improves with the value of the inertance b, with the height of the location where the TID is installed and with the distance L between the two TID attachment locations along the tower height.
- The maximum stroke of the TID is within 0.3–0.4 m, which makes the TID suitable for installation in the tower of the WT.
- The performance improvements brought by the TID do not change significantly with the time instant of earthquake occurrence and remain significant no matter when the earthquake occurs into the simulation.
- A comparison with the performance of a 35 t TMD installed in the tower top/nacelle shows that a TID always outperforms the TMD.

Further work will aim at overcoming some simplifying yet reasonable and well-established assumptions made, in this study, on the operational thrust force modelling and on the structural FE model. Firstly, future developments will aim at assessing the performances of the TID via time-domain fully-coupled aero-servo-elastic simulations,

where the rotor aerodynamics may be accurately modelled under simultaneous wind and earthquake actions. This will also provide the opportunity to assess the potential of the TID to mitigate the effects of a possible emergency rotor shutdown triggered by the earthquake excitation. Secondly, based on the stress resultants obtained from the fully-coupled aero-servo-elastic simulations, refined FE models of structural members, including TID components, could be implemented using 2D/3D FEs for detailed structural analysis.

On the other hand, further work is warranted to study multi-axis TIDs under multi-directional excitations, as well as applications to offshore WTs. These extensions are left for future work.

Declaration of Competing Interest

The authors declare that they have no known competing financial interests or personal relationships that could have appeared to influence the work reported in this paper.

Acknowledgements

Author G. Alotta gratefully acknowledges the financial support from the project PON-AIM 1805501-2 (Line 1), financed by the Italian Minister of University and Research (MIUR).

Author G. Failla gratefully acknowledges the financial support from the Italian Ministry of Education, University and Research (MIUR), under the PRIN 2017 National Grant “Multiscale Innovative Materials and Structures” (grant number 2017J4EAYB).

Author A. Giaralis gratefully acknowledges the support of Royal Academy of Engineering in UK through the Industrial Fellowship grant IF2223-209 (OPTWIND project).

References

[1] Ma Y, Martinez-Vazquez P, Baniotopoulos C. Wind turbine tower collapse cases: a historical overview. Proc Inst Civ Eng - Struct Build 2019;172(8):547–55.
[2] Fitzgerald B, Basu B. Vibration control of wind turbines: recent advances and emerging trends. Int J Sust Mater Struct Syst 2020;4(2/3/4):347–72.
[3] Malliotakis G, Alevras P, Baniotopoulos C. Recent advances in vibration control methods for wind turbine towers. Energies 2021;14(22):7536.
[4] Stamatopoulos GN. Response of a wind turbine subjected to near-fault excitation and comparison with the Greek Aseismic Code provisions. Soil Dyn Earthq Eng 2013;46:77–84.
[5] Díaz O, Suárez LE. Seismic analysis of wind turbines. Earthq Spectra 2014;30(2):743–65.
[6] Prowell I, Uang C-M, Elgamal A, Luco JE, Guo L. Shake table testing of a utility-scale wind turbine. J Eng Mech 2012;138(7):900–9.
[7] Stewart GM, Lackner MA. The impact of passive tuned mass dampers and wind–wave misalignment on offshore wind turbine loads. Eng Struct 2014;73:54–61.
[8] Ghassempour M, Failla G, Arena F. Vibration mitigation in offshore wind turbines via tuned mass damper. Eng Struct 2019;183:610–36.
[9] Gaur S, Elias S, Höbbel T, Matsagar VA, Thiele K. Tuned mass dampers in wind response control of wind turbine with soil-structure interaction. Soil Dyn Earthq Eng 2020;132:106071.
[10] Mensah AF, Dueñas-Osorio L. Improved reliability of wind turbine towers with tuned liquid column dampers (TLCDs). Struct Saf 2014;47:78–86.
[11] Ding H, Chen Y-N, Wang J-T, Altay O. Numerical analysis of passive toroidal tuned liquid column dampers for the vibration control of monopile wind turbines using FVM and FEM. Ocean Eng 2022;247:110637.
[12] Ollgaard B, Jensen SP. Wind turbine tower having a damper. US Patent 9. 2017;657:717.
[13] Sun C, Jahangiri V. Bi-directional vibration control of offshore wind turbines using a 3D pendulum tuned mass damper. Mech Syst Signal Pr 2018;105:338–60.
[14] Bertollucci Colherinhas G, Petrini F, Morais MVG, Bontempi F. Optimal design of passive-adaptive pendulum tuned mass damper for the global vibration control of offshore wind turbines. Wind Energy 2021;24(6):573–95.
[15] Zuo H, Bi K, Hao H. Using multiple tuned mass dampers to control offshore wind turbine vibrations under multiple hazards. Eng Struct 2017;141:303–15.
[16] Hu Y, Wang J, Chen M, Li Z, Sun Y. Load mitigation for a barge-type floating offshore wind turbine via inerter-based passive structural control. Eng Struct 2018;177:198–209.
[17] Zhang R, Zhao Z, Dai K. Seismic response mitigation of a wind turbine tower using a tuned parallel inerter mass system. Eng Struct 2019;180:29–39.
[18] Sarkar S, Fitzgerald B. Vibration control of spar-type floating offshore wind turbine towers using a tuned mass-damper-inerter. Struct Control Hlth 2020;27(1):e2471.
[19] Smith MC. Synthesis of mechanical networks: the inerter. IEEE Trans Automat Contr 2002;47(10):1648–62.
[20] Watanabe Y, Ikago K, Inoue N, Kida H, Nakaminami S, Tanaka H, Sugimura Y, Saito K. Full-scale dynamic tests and analytical verification of a force-restricted tuned viscous mass damper. Proceedings of the 15th World Conference on Earthquake Engineering, Lisbon, Portugal, 2012.
[21] Nakaminami S, Kida H, Ikago K, Inoue N. Dynamic testing of a full-scale hydraulic inerter-damper for the seismic protection of civil structures, in: M. Furinghetti, D. Bolognini, A. Pavese (Eds.). Proceedings of the 7th International Conference on Advances in Experimental Structural Engineering, 2017, Eucentre Foundation, Pavia, Italy, 2017, 41-54.
[22] Alotta G, Failla G. Improved inerter-based vibration absorbers. Int J Mech Sci 2021;192:106087.
[23] Ikago K, Saito K, Inoue N. Seismic control of single-degree-of-freedom structure using tuned viscous mass damper. Earthq Eng Struct Dyn 2012;41(3):453–74.
[24] Garrido H, Curadelli O, Ambrosini D. Improvement of tuned mass damper by using rotational inertia through tuned viscous mass damper. Eng Struct 2013;56:2149–53.
[25] Zhang R, Cao Y, Dai K. Response control of wind turbines with ungrounded tuned mass inerter system (TMIS) under wind loads. Wind Struct 2021;32(6):573–86.
[26] Zhang Z, Høeg C. Inerter-enhanced tuned mass damper for vibration damping of floating offshore wind turbines. Ocean Eng 2021;223:108663.
[27] Jonkman J, Butterfield S, Musial W, Scott G. Definition of a 5-MW reference wind turbine for offshore system development. In: Technical report NREL/TP-500-38060, National Renewable Energy Laboratory, Golden, CO, 2009.
[28] Chen MZQ, Li Z, Wang H, Hu Y. Seismic response mitigation of a wind turbine via inerter-based structural control. Bull Earthq Eng 2023;21(3):1361–88.
[29] Lazar IF, Neild SA, Wagg DJ. Using an inerter-based device for structural vibration suppression. Earthq Eng Struct Dyn 2014;43(8):1129–47.
[30] Marian L, Giaralis A. Optimal design of a novel tuned mass-damper-inerter (TMDI) passive vibration control configuration for stochastically support-excited structural systems. Prob Eng Mech 2014;38:156–64.
[31] Ruiz R, Taflanidis AA, Giaralis A, Lopez-Garcia D. Risk-informed optimization of the tuned mass-damper-inerter (TMDI) for the seismic protection of multi-storey building structures. Eng Struct 2018;177:836–50.
[32] Patsialis D, Taflanidis AA, Giaralis A. Tuned-mass-damper-inerter optimal design and performance assessment for multi-storey hysteretic buildings under seismic excitation. Bull Earthq Eng 2023;21(3):1541–76.
[33] Petrini F, Giaralis A, Wang Z. Optimal tuned mass-damper-inerter (TMDI) design in wind-excited tall buildings for occupants' comfort serviceability performance and energy harvesting. Eng Struct 2020;204:109904.
[34] Wang Z, Giaralis A. Top-story softening for enhanced mitigation of vortex shedding-induced vibrations in wind-excited tuned mass damper inerter-equipped tall buildings. J Struct Eng 2021;147(1):04020283.
[35] Dai J, Xu ZD, Gai PP. Tuned mass-damper-inerter control of wind-induced vibration of flexible structures based on inerter location. Eng Struct 2019;199:109585.
[36] Xu T, Li Y, Leng D. Mitigating jacket offshore platform vibration under earthquake and ocean waves utilizing tuned inerter damper. Bull Earthq Eng 2023;21(3):1627–50.
[37] SAP2000 v.24, Computers and Structures Inc.
[38] Alati N, Failla G, Arena F. Seismic analysis of offshore wind turbines on bottom fixed support structures. Phil Trans R Soc A 2015;373(2035):20140086.
[39] Asareh MA, Schonberg W, Volz J. Fragility analysis of a 5-MW NREL wind turbine considering aero-elastic and seismic interaction using finite element method. Finite Elem Anal Des 2016;120:57–67.
[40] Santangelo F, Failla G, Santini A, Arena F. Time-domain uncoupled analyses for seismic assessment of land-based wind turbines. Eng Struct 2016;123:275–99.
[41] Giaralis A, Taflanidis AA. Optimal tuned mass-damper-inerter (TMDI) design for seismically excited MDOF structures with model uncertainties based on reliability criteria. Struct Control Hlth 2018;25(2):e2082.
[42] Wang Z, Giaralis A. Enhanced motion control performance of the tuned mass damper inerter through primary structure shaping. Struct Control Hlth 2021;28(8):e2756.
[43] Ali A, De Risi R, Sextos A. Seismic assessment of wind turbines: how crucial is rotor-nacelle-assembly numerical modeling? Soil Dyn Earthq Eng 2021;141:106483.
[44] Den Hartog JP. Mechanical vibrations. New York, NY: McGraw-Hill Inc; 1947.
[45] Krenk S. Frequency analysis of the tuned mass damper. J Appl Mech 2005;72(6):936–42.
[46] Rana R, Soong TT. Parametric study and simplified design of tuned mass dampers. Eng Struct 1998;20(3):193–204.
[47] Krenk S. Resonant inerter based vibration absorbers on flexible structures. J Frankl Inst 2019;356(14):7704–30.
[48] Ali A, De Risi R, Sextos A, Goda K, Chang Z. Seismic vulnerability of offshore wind turbines to pulse and non-pulse records. Earthq Eng Struct Dyn 2020;49(1):24–50.
[49] Muskulus M. Simplified rotor load models and fatigue damage estimates for offshore wind turbines. Phil Trans Roy Soc A 2015;373(2035):20140347.
[50] Karimirad M, Moan T. A simplified method for coupled analysis of floating offshore wind turbines. Mar Struct 2012;27(1):45–63.
[51] Wang L, Sweetman B. Simulation of large-amplitude motion of floating wind turbines using conservation of momentum. Ocean Eng 2012;42:155–64.
[52] Valamanesh V, Myers A. Aerodynamic damping and seismic response of horizontal axis wind turbine towers. J Struct Eng 2014;140(11):04014090.
[53] Santangelo F, Failla G, Arena F, Ruzzo C. On time-domain uncoupled analyses for offshore wind turbines under seismic loads. Bull Earthq Eng 2018;16(2):1007–40.

[54] Shinozuka M. Monte Carlo solution of structural dynamics. Comput Struct 1972;2 (5–6):855–74.
[55] International Electrotechnical Commission. Standard: IEC 61400-1 wind turbines part 1: requirements, 2015.
[56] Sobhaniasl M, Petrini F, Karimirad M, Bontempi F. Fatigue life assessment for power cables in floating offshore wind turbines. Energies 2020;13:3096.
[57] Al-Solihat MK, Nahon M. Flexible multibody dynamic modeling of a floating wind turbine. Int J Mech Sci 2018;142–143:518–29.
[58] Laface V, Alotta G, Failla G, Ruzzo C, Arena F. A two-degree-of-freedom tuned mass damper for offshore wind turbines on floating spar supports. Mar Struct 2022;83: 103146.
[59] Pacific Earthquake Engineering Research Center (PEER). Peer ground motion database. Berkeley: University of California; 2013. http://ngawest2.berkeley.edu/.
[60] Sigurðsson GÖ, Rupakhety R, Rahimi SE, Olafsson S. Effect of pulse-like near-fault ground motions on utility-scale land-based wind turbines. Bull Earthq Eng 2020;18 (3):953–68.